Review

A Comprehensive Review on Catalytic Activities of Green-Synthesized Selenium Nanoparticles on Dye Removal for Wastewater Treatment

Amin Barani [ID], Seyedeh Roya Alizadeh and Mohammad Ali Ebrahimzadeh *[ID]

Department of Medicinal Chemistry, School of Pharmacy and Pharmaceutical Sciences Research Center, Mazandaran University of Medical Sciences, Sari 48471-93698, Iran; a.barani1995@gmail.com (A.B.); r.alizadeh.2019@gmail.com (S.R.A.)
* Correspondence: zadeh20@gmail.com

Abstract: The increase in economic activities and the industrialization of countries have caused the growth of pollution created by waste and sewage. In particular, the textile industry produces large amounts of liquid contaminants due to the large amounts of water employed during the production of fabrics. In addition, dyes are another category of organic compound used in many industries, such as pharmaceuticals and rubber making. The presence of limitations in physico-chemical methods for the degradation of various dyes has stimulated the interest of researchers worldwide. One of the most economical ways is the use of photocatalytic decomposition under UV light radiation by green nanoparticles (NPs). In recent years, various metal NPs have been made using the green method that is cost-effective, eco-friendly, safe, and simple. Selenium (Se) is a crucial semiconductor metal that is widely utilized for its outstanding photovoltaic and optoelectronic attributes. Due to the excellent physical characteristics of Se, such as thermo-conductivity, anisotropy, and high photoconductivity, it has been used for removing various organic dyes. Hence, green SeNPs have attracted much attention in the catalytic decomposition process. The current review focuses on providing comprehensive studies concerning the degradation or reduction of various organic dyes through green SeNPs as an effective and efficient method and their mechanisms. It highlights the importance of utilizing green chemistry and catalytic properties. The aim is to benefit researchers from both academic and industrial backgrounds.

Keywords: green selenium nanoparticles; wastewater treatment; photocatalysis; dye degradation

1. Introduction

Due to the rapid growth of the population and the rapid increase in the industrialization of cities, environmental pollution has been raised as a major global problem [1,2]. Chemical industrial wastewater contains toxic substances, such as dyes, heavy metals, and organic pollutants [3,4]. Among the types of water pollution, dyes are the main forms of waste and harmful substances that enter the water. Every year, various dyes are produced by various industries, such as the cosmetic, plastic, leather, hair dye, textile, photoelectrochemical cell, paper, agricultural research, pharmaceutical, and food industries [3]. Statistics indicate that about 1.2 billion people do not have access to safe drinking water, and millions of people die from consuming contaminated water [5]. Observations and research showed that dyes are usually carcinogenic [6], mutagenic, and teratogenic and have a harmful nature.

In humans, some dyes can cause bladder cancer, skin irritation, nausea, vomiting, gastrointestinal irritation, and disorders of the liver, brain, kidneys, and central nervous system [2,7,8]. The risk of dyes for the environment and natural ecosystems depends on environmental exposure (concentration and duration) and potential contamination (hazard

or toxicity characteristics). Only the presence of 1 mg/L of dye in drinking water can lead to significant health concerns for humans [3].

There are various methods to remove different dyes from the natural ecosystem, including the physical removal of dyes (adsorption, filtration, sedimentation, and reverse osmosis), chemical decolorization (chemical oxidation, neutralization, ion exchange, and recovery methods), and biological methods (degradation using fungi, bacteria, and actinomycetes). Disadvantages of physical and chemical methods include high operating costs and the production of toxic sludge. In addition, biological methods have some problems, including a long time for dye decomposition, low decomposition efficiency, high structural stability of some dyes, and resistance to bacterial degradation [7]. In addition, dyes in wastewater usually have one or more benzene rings that cannot be easily removed by biological and chemical methods to decompose [1]. As a result, we need an optimal, cost-effective, high-efficiency, and environmentally friendly method to remove dyes and pollution [9]. Photocatalysis is an "advanced oxidation process (AOP)" using ultraviolet or visible light, which has been proposed as a cost-effective, efficient, and eco-friendly method. It involves the use of metal-based nanoparticles [10]. In this method, organic pollutants are broken down into smaller molecules or completely decomposed into CO_2 and H_2O [11].

Nanotechnology deals with nanoscale objects. The surface-to-volume ratio has increased in nanoparticles, and therefore, they exhibit unique optical, magnetic, catalytic, and electrical properties [12,13]. Nanoparticles are utilized in different fields, such as toxic gas sensing, heavy metal removal, textile applications, and the biomedical and photocatalytic degradation of organic pollutants [14–18]. In general, there are two methods for the production of nanoparticles, which comprise "the top-down and bottom-up approaches". The top-down approach includes physical methods, such as vapor deposition, ball milling, and laser ablation. The bottom-up approach contains chemical methods (sol-gel, pyrolysis, solvothermal, and microwave irradiation) and biological methods (microorganisms or plant extracts) [3,19]. Among these methods, physical and chemical methods are less used compared to biological methods due to the high cost and residual toxic solvents, but the green synthesis method with a plant is economical, environmentally friendly, safe, and simple [20]. When natural organic matter is present in the environment, it has the ability to be adsorbed onto the NPs, resulting in a reduction of their agglomeration. Furthermore, this adsorption process can decrease their toxicity [21]. In fact, the green method generates more stable and less toxic products than those obtained using other methods [22]. In recent years, various nanoparticles, such as CuO [23], TiO_2 [24], ZnO [25], MgO [26], Pt [27], Ag [28], Au [29], Fe [30], and Se [31], were synthesized using the green method. They showed potential anticancer, antimicrobial, antifungal, and photocatalytic activities.

Selenium (Se) is an essential element for the human body as well as for animals. Its absence can result in permanent and severe conditions, including immune deficiency. It has been noted that this particular substance is present in certain functional proteins that are responsible for crucial tasks like promoting anticancer properties and enhancing the immune system to combat harmful agents. Selenium has been observed to significantly affect membrane peroxidases by reacting with them and producing oxygen-free radicals, ultimately leading to antimicrobial effects. In addition, semiconductor chalcogens, such as Se, have been utilized for the removal of various dye groups owing to their superior physical attributes, including "thermo-conductivity, anisotropy, and high photoconductivity" [32,33]. In fact, Se, as a notable semiconductor, is extensively utilized for its photovoltaic and optoelectronic properties [34]. The remarkable position of Selenium nanoparticles (SeNPs) can be explained by the interest invested in their synthesis due to their distinctive properties, which has led to the various methods currently being evaluated [35]. Different types of plants and microorganisms possess the ability to convert selenite [Se(IV)] to Se(0) and generate extracellular or intracellular SeNPs. Bio-SeNPs have found diverse applications as an eco-friendly and green nanomaterial in several areas, such as anticancer and antimicrobial activities, drug delivery, and nutritional supplements [36]. The green SeNPs exhibit remarkable biomedical characteristics and demonstrate superior biocompatibility

and degradability in comparison to alternative metal nanoparticles [37]. Biogenic Se nanomaterials have been utilized as adsorbents for Hg (0), Zn^{2+}, Cu^{2+}, and Cd^{2+} due to their high affinity for certain heavy metals. Furthermore, Se nanomaterials possess a bandgap of 1.99 eV (amorphous Se) or 1.8 eV (crystalline Se), which suggests that they have the potential to be highly efficient photocatalysts. The photocatalytic decomposition of Methylene blue in aqueous media with gum shellac stabilized SeNPs was described by Iqbal et al. [38]. Velayati evaluated the photocatalytic effect of Gum arabic mediated-Se-Nanorods on the degradation of Rhodamine B dye under a UV-A light [35]. The photocatalytic degradation of Bromothymol blue using biogenic SeNPs prepared by terrestrial actinomycete Streptomyces griseobrunneus strain FSHH12 was reported by Ameri et al. [32]. Many studies have reported the ability of green synthesized SeNPs on organic dye degradation, which is related to the special properties of SeNPs. Hence, this review article has investigated the photocatalytic effects of green SeNPs in the degradation or reduction of some organic dyes, considering the importance of organic dyes as environmental pollutants and their removal using the best method (Figure 1).
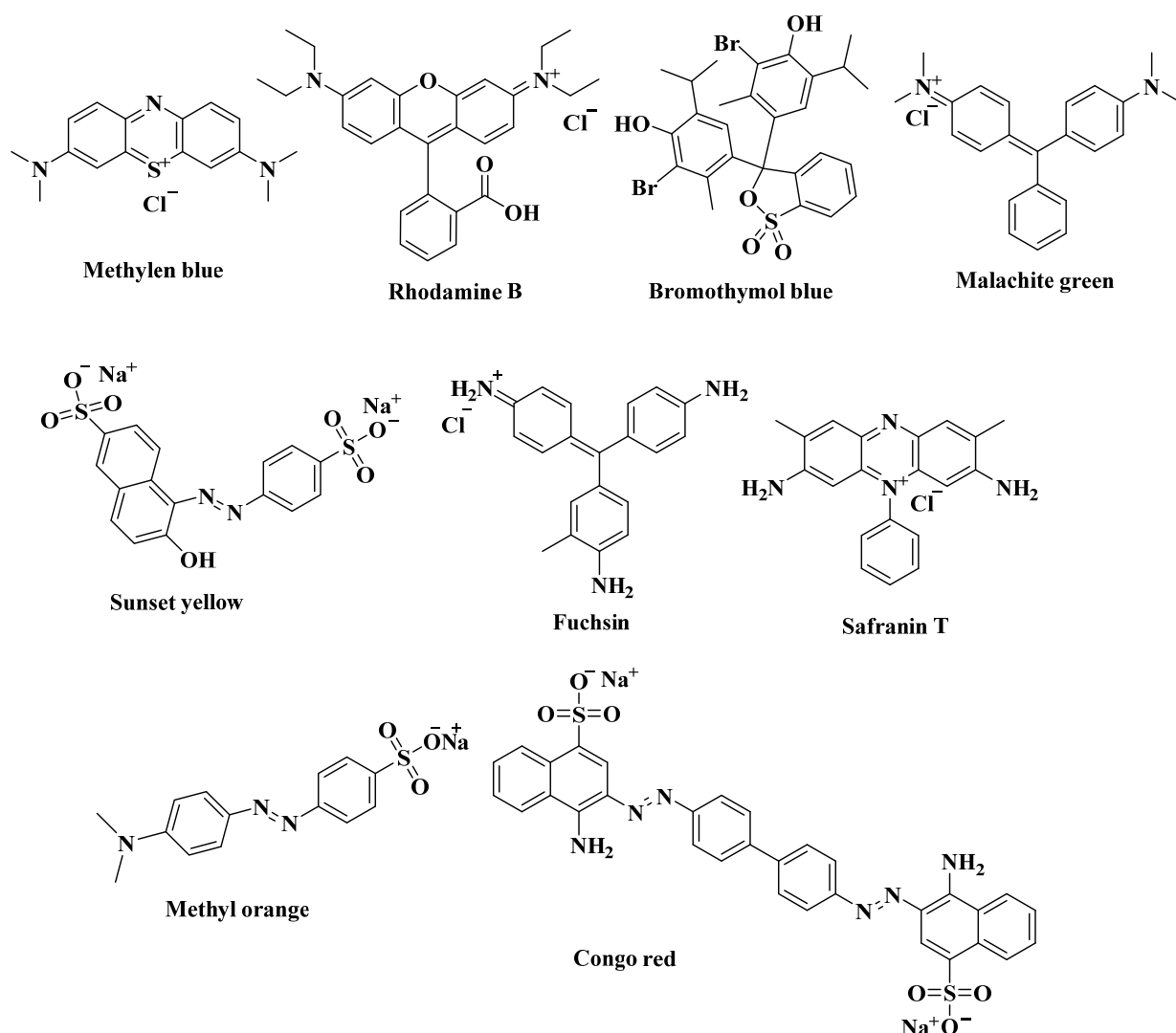

Figure 1. The structure of several organic dyes.

2. Several Organic Pollutants Dyes (Table 1)

2.1. Methylene Blue

Methylene blue (MB) is a pollutant with a thiazine structure, which is highly carcinogenic and mutagenic, and is used in many different factories (dyeing paper, cotton,

etc.). Consumption of this substance causes toxicity and serious damage to the eyes and nervous system. In addition, MB showed some complications, such as respiratory infection, digestive problems, nausea, and vomiting [39,40]. Therefore, MB is a serious threat to the health of humans and animals; hence, a proper method must be used to eliminate this harmful substance. It is easy to document and check the progress of the photocatalytic reaction because MB dye disappears due to the degradation in the reaction medium. In addition, MB is a dark blue solid powder at room temperature, which is soluble in water, and its maximum optical absorption is observed at 665 nm. The absorption peaks of MB observed by a UV–Vis spectrophotometer decrease or disappear during the photocatalytic process [41,42]. Several studies investigated the degradation of MB using green SeNPs.

Green SeNPs were synthesized using fermented yeast based on agricultural waste by Goud et al., in 2016 [34]. These nanoparticles were identified using diagnostic methods, such as UV–Vis (540 nm), SEM, EDX, XRD, and DSC. The average size of the synthesized rod-shaped nanoparticles was between 240 and 170 nm. The crystalline nature of SeNPs was proven with XRD studies. The EDX profile exhibited that the major component is Se while other elemental signals (carbon, oxygen, nitrogen, phosphorus, and sulphur peaks) may originated from phytochemicals or proteins existing in fermented broth. In order to study the photocatalytic effect, 50 mg of SeNPs were added to 50 mL of MB (10 mg/L) under visible light "(a visible annular type photoreactor with 300 W tungsten lamp)", and it was checked for 3 h. Furthermore, the fabricated nanoparticles had significant anticancer and antibacterial effects [34].

In the other study published in 2018, Venkatesan and coworker [43] prepared green SeNPs with a leaf extract of *Withania somnifera* and selenious acid (H_2SeO_3). FT-IR analysis confirmed the presence of functional groups, which were associated with bioactive molecules in the extract; the result was consistent with the stability of the colloidal solution of nanoparticles. It was found that the synthesized SeNPs were amorphous and spherical within the diameter range of 45–90 nm. The X-ray pattern was indexed based on the trigonal phase of Se. The bandgap energy for the as-prepared sample was determined to be 2.75 eV after 24 h of aging. It was noted that the bandgap energy of green SeNPs was greater than that of bulk α-Se (2.0 eV) and commercial Se powder (1.8 eV) owing to the quantum size effect. The reference peak for MB was in the region of 657 nm, and it was examined during 0–30 min period. The maximum amount of decolorization effect was determined after 30 min in the presence of sunlight. SeNPs have the ability to effectively degrade MB in the presence of sunlight, making them suitable for use in "water treatment plants and textile industries". In addition, the synthesized SeNPs showed antioxidant, antimicrobial, and antiproliferative effects [43].

Xia et al., in 2019, [44] utilized a green approach to synthesize SeNPs and assessed their potential for a photocatalytic effect in the presence of MB under visible light "(a 300 W Xe lamp ($\lambda > 400$ nm) to simulate the visible-light)". Sodium formaldehyde sulfoxylate was utilized as the reducing agent for the synthesis of trigonometric Se nanowires from SeO_2 with diameters ranging from 100 to 200 nm. The calculated bandgap energy of the SeNPs, as prepared, was determined to be 1.52 eV, which is slightly lower than the bandgap of bulk Se at 1.6 eV. The prepared SeNPs exhibited a good catalytic effect by degrading more than 99% of MB (664 nm) after 3 h in the presence of H_2O_2 [44].

Tripathi and colleagues [45] fabricated SeNPs through cost-effective methods and away from the disadvantages of chemical methods using the leaf extract of *Ficus benghalensis*. The precursors were Se metal powder and sodium sulphide. The size distribution range of the particles was 45–95 nm with a spherical shape; the average particle size was 64.03 nm, which was measured with DLS and SEM methods. Based on the XRD pattern, the nanoparticles were polycrystalline in nature. The bandgap of biosynthesized SeNPs is higher compared to that of commercial Se powder, with a value of 3.8 eV. This phenomenon is attributed to quantum confinement as well as the probable influence of capping ligands and proteins present on the surface of nanomaterials. The concentration of 10 mg/L of MB and 100 mg/L of SeNPs was used for the photocatalytic investigations under UV irradiation. MB had two

peaks in the region of 619 and 664 nm in UV–Vis, and the peak at 664 nm was selected as a reference. The MB degradation followed first-order kinetics and had a rate constant of 0.02162 s^{-1}, resulting in a degradation of 57.63% after 40 min of reaction time [45].

A fungal extract called *Monascus purpureus* ATCC16436 was used to form green SeNPs. Sodium selenite (Na_2SeO_3) was used as a Se precursor. The synthesis of nanoparticles was approved by UV–Vis after 30 min at room temperature. The prepared SeNPs appeared in a single-phase crystalline structure. TEM image discovered the round form with a mean particle size of 46.58 nm. DLS analysis showed that the prepared SeNPs had been monodispersed with a polydispersity index value of 0.205. The zeta potential of -24.01 mV exhibited the high stability of synthesized SeNPs. In order to investigate the photocatalytic effect, 25–400 mg of SeNPs were added to 100 mL of MB (10 mg/L) under sunlight and checked for 20 min. A progressive increase in the degradation percentage was obtained with the increase within the SeNPs concentrations, which reached the greatest degradation (100%) at 4 mg/mL SeNPs. In addition, SeNPs showed effective antimicrobial activity against all plant and human pathogens, antioxidants, and anticancer activities [46].

In another study published in 2021 by Kazemi et al., [47] SeNPs were green synthesized using Na_2SeO_3, glucose, and ascorbic acid (AA), in which way starch had the role of stabilizer and capping agent. SeNPs were characterized by several procedures, including UV–Vis, XRD, AFM, DLS, XRD, FE-SEM, and TEM. The TEM image of NPs demonstrated a spherical form that was effectively distributed on the starch stabilizer and contained a diameter within the size range of 2–10 nm. The XRD of SeNPs showed a clear pattern with an average crystalline size of 20 nm. After exposure to UV-A light, the bandgap energy was determined to be 5.12 eV. It was observed that the synthesized SeNPs had a greater bandgap energy than the bulk material (2.5 eV), which can be attributed to the quantum size effect. In order to investigate the photocatalytic effect, 20 mL of SeNPs (0.01 mmol) and 5 mL of MB (0.1 mmol) were used for 0–150 min. The rate constant was determined to be 0.015 min^{-1}, and MB (60%) decomposed under UV light after 150 min. It is important that there is no indication of dye degradation during the loss of catalysts or in the absence of UV irradiation. The utilization of a pseudo-first-order reaction has appeared to be suitable for estimation purposes. SeNPs showed satisfactory activity in the antimicrobial and photocatalytic cases [47].

In a study by Cittrarasu et al. (2021), [48] SeNPs were synthesized with an aqueous extract of *Ceropegia bulbosa* tuber and selenous acid. The characterization of the synthesized SeNPs was conducted with FT-IR mapping, XRD, FE-SEM-EDS, HR-TEM, DLS, and zeta potential analysis. FE-SEM and HR-TEM found that the shape of the nanoparticles was uniformly spherical. The DLS results of SeNPs showed an average size of 55.9 nm with a dispersion index of 0.03. Aqueous solution mediated by SeNPs can degrade 98.3% MB in 80 min. The efficiency of MB decolonization was observed to steadily increase with a longer period of irradiation time, up to a maximum of 80 min [48].

Santhosh and colleagues (2022) [37] produced *Goniothalamus wightii* extract-mediated SeNPs. In addition, Na_2SeO_3 and AA were used during the synthesis. Prepared SeNPs were confirmed through EDX, UV–Vis, TEM, SEM, and FT-IR. The average size of the produced nanoparticles was 80 nm. The XRD pattern revealed a highly crystalline structure. Zeta potential and DLS value of synthesized SeNPs were determined as -17.6 mV and 20–110 nm. To examine the photocatalytic effect, 10 mg of SeNPs were added to 100 mL of MB (10 mg/L) under sunlight, and dye decomposition was checked at 660 nm every 30 min. The prepared SeNPs were able to decompose 97% of MB dye in 150 min. In addition, these nanoparticles displayed radical scavenging, anticancer, and photocatalytic activities [37].

Alizadeh and colleagues (2023) [49] prepared green SeNPs mediated from the aqueous extract of *Allium paradoxum* and Na_2SeO_3. Several analytical methods (FT-IR, TGA, XRD, EDX, SEM, and TEM) proved the synthesis of SeNPs. These nanoparticles with a semi-spherical shape and an average size of 37.5 nm exhibited a good photocatalytic effect in the removal of MB dye in the presence of $NaBH_4$ (reducing agent); 30 μL of MB (10 mM), 5.77 mL H_2O, and 200 μL of fresh $NaBH_4$ (0.1 M) were treated with 50, 60, and 70 μL

of SeNPs (700 µg/mL). The complete degradation efficiency was obtained after 69, 49, and 41 min, and the rate constants were calculated as 0.0198, 0.0199, and 0.0361 min^{-1}, respectively. The photocatalytic reaction was pseudo-first-order kinetics. The green SeNPs had antioxidant, antibacterial, iron-chelating, anticancer, antifungal, and photocatalytic activities [49].

In another study by Alizadeh et al. (2023), [50] green synthesis of SeNPs was performed using the aqueous extract of *Crocus caspius* plant and Na$_2$SeO$_3$. They had a crystalline nature (triangular) with a semi-spherical shape and an average size of 20.34 nm. The green SeNPs showed strong radical inhibitory, antibacterial, iron chelating, anticancer, antifungal, antileishmanial, and photocatalytic activities. The fabricated nanoparticles displayed a good photocatalytic effect in the removal of MB dye in the presence of NaBH$_4$, so the reduction rates of 0.1474, 0.1538, and 0.1625 min^{-1} were obtained for 40, 50, and 60 µL of SeNPs (546.67 µg/mL), respectively. The photocatalytic reaction was determined by pseudo-first-order kinetics [50].

Ebrahimzadeh and colleagues (2023), [51] synthesized SeNPs using Na$_2$SeO$_3$ and the aqueous extract of *Hibiscus esculentus* L. and confirmed their capping and synthesis by instrumental analysis. They were in the form of hexagonal crystals and spherical shapes with a size of 62 nm. To explore the photocatalytic effect, a 200 µL NaBH$_4$ (0.1 M) solution, 5.77 mL H$_2$O, and 30 µL of MB (10 mM) were mixed with 70 µL of colloidal SeNPs (1110 µg/mL). The prepared SeNPs nanoparticles can degrade MB dye in 21 min at 665 nm to the extent of 98.3% with a rate constant of 0.1023 min^{-1} in the presence of NaBH$_4$ by pseudo-first-order kinetics [51].

Velayutham et al. [52] utilized an eco-friendly method to produce bio-NiSeNPs through the use of *Hibiscus rosa-sinensis* extract. A hydrothermal technique was employed to combine the NiSeNPs. UV–Visible spectroscopy was employed to verify the reduction and stabilization of Ni^{2+} and Se^{2-} ions, forming NiSeNPs with a bandgap of 1.74 eV. This facilitates the production of electrons and holes on the surface of the NPs. XRD pattern exhibited the crystallite size of 24 nm. The micrographs observed through FE-SEM and TEM demonstrated a spherical shape with an average size of 26 nm. FT-IR spectroscopy confirmed the presence of functional groups on the surface of NiSeNPs and showed surface interactions with bio-materials in the extracts. The XPS analysis was able to provide some information regarding the chemical composition, Ni and Se valency, and their interface. The prepared NiSeNPs had a bandgap of 1.74 eV. The efficacy of the NiSeNPs in photodegrading MB dye led to a 92% degradation under visible light. Moreover, the NiSeNPs displayed bactericidal properties against *Escherichia coli* and *Staphylococcus aureus* strains as a result of the sophisticated oxidation and reduction of charged NPs, which amplified the degradation ability and hindered cell proliferation [52].

Thin hexagonal sheets of Cu$_2$Se with large dimensions were successfully synthesized through a convenient green approach utilizing AA (reduction agent) and β-CD (surfactant). The formation of the Cu$_2$Se hexagonal sheets was proposed to follow a "Nucleation-Triangle-Hexagonal" mechanism. The ultimate morphology of the Cu$_2$Se hexagonal sheets was discovered through the combined influence of β-CD and the growth rates of various crystal planes. The bandgap value of Cu$_2$Se was evaluated 2.25 eV. The Cu$_2$Se hexagonal sheets exhibited remarkable capabilities for adsorption and photocatalysis when exposed to visible light. In the presence of H$_2$O$_2$, these sheets can degrade up to 99% of MB within just one hour [53].

Nouri's team [54] synthesized Cu$_2$Se$_3$ nanostructures and copper selenide/graphene nanocomposites using glycine amino acid (Gly) (green surfactant) and graphene oxide (GO) sheets (graphene source). The XRD analysis of the products revealed that they were Cu$_2$Se$_3$ with a tetragonal phase. Based on SEM and TEM images, the NPs decorating the rGO sheets were significantly smaller in size compared to the pristine NPs. The pristine Cu$_3$Se$_2$ exhibited a dendritic morphology, with particles being intricately decorated on the leaves. Furthermore, the UV–Vis results indicated that the absorption peak of the products fell within the visible region with a bandgap value ranging from 1.85 eV to 1.95 eV. Finally, the

prepared compounds were utilized as photocatalytic materials for the purpose of removing MB dye under both solar and visible light irradiations. It was discovered that rGO played a crucial role in enhancing the photocatalytic performance of the products, and Cu_2Se_3/rGO (15%) was able to degrade MB (91% and 73%) within one hour under solar and visible lights, respectively [54].

Saray et al. [55] produced "CuxSey@polyaniline core-shell nanocomposites" (CuxSey/PANI) as photocatalytic materials that exhibit exceptional performance when exposed to visible light irradiation. Additionally, the SEM and TEM images provided that the disk-shaped pristine CuxSey nanostructures transformed into NP morphology, with an average diameter of approximately 25 nm. The outcomes of the photocatalytic tests revealed that PANI played a vital role in enhancing the photocatalytic efficiency of the CuxSey nanostructures in a synergistic manner with the optimal concentration of 10% for PANI. CuxSey/PANI (10%) nanocomposites degraded nearly 100% of MB dye in only 75 min. The characterization techniques revealed that PANI had a positive impact on the porosity of nanocomposites and concurrently generated a type-II heterostructure with CuxSey nanostructures. Therefore, PANI plays a vital role as a synergistic factor in the photocatalytic process by enhancing the absorption of additional photons and suppressing the recombination of electron-holes formed in the nanocomposite [55].

2.2. Rhodamine B

Rhodamine B (RhB) is one of the most toxic dyes in the wastewater of textile industries because of its high stability and non-biodegradability. The maximum UV–Vis absorption peak of RhB is observed at 554 nm. During photocatalysis, the intensity of this peak should decrease, and it can be observed a blue shift, which indicates de-ethylation [56]. RhB is a cationic dye with high solubility in water. It is highly carcinogenic, mutagenic, and neurotoxic. Studies have shown that it causes respiratory problems, hemolysis, eye infections, degenerative changes in the liver and kidney, and the death of planktons. In addition, RhB dye prevents the penetration of light into the water and reduces photosynthesis; therefore, it is ultimately a threat to aquatic life. Like other dyes, this dye is resistant to heat, light, oxidation, and biological decomposition [57,58].

Che et al. [59] discovered that the sulfite reductase enzyme in *Lysinibacillus* sp. ZYM-1 can convert Na_2SeO_3 into SeNPs. The size of these nanoparticles was found to be 100–200 nm. When the concentration increases from 1 to 25 mM, the morphology of the synthesized particles changes from cubic to spherical. The spherical amorphous SeNPs were compared with triangular SeNPs in investigating the photocatalytic effect. The rate of photocatalytic decomposition of RhB under visible light with H_2O_2 was checked after 300 min, and it was found that the rate of photocatalytic decomposition of spherical nanoparticles (0.0048 min^{-1}) was higher than that of triangular nanoparticles (0.0011 min^{-1}). Two possible mechanisms for RhB degradation were determined using LC-HRMS "(liquid chromatography-high resolution mass spectrometry)", including N-de-ethylation and the conjugated chromophore structure cleavage [59].

In 2019, Kazemi and coworkers [60] were able to synthesize SeNPs using a green method; sodium salt of Na_2SeO_3 was used as a source of Se, gelatin as a coating, and glucose and AA as a green reducing agent. In fact, gelatin was utilized as a stabilizing agent owing to its capability to combine and bind with Na_2SeO_3, which can subsequently be transformed into insoluble elemental Se in situ by the use of glucose. As a result, the gelatin molecules can be viewed as the optimal surfaces for Se particles, which can also regulate their growth. Green SeNPs were identified using XRD, UV–Vis, DLS, TEM, FE-SEM, EDX, and ATM analysis. The synthesized SeNPs had a hexagonal crystal structure and spherical shape with an average size of less than 20 nm. Through the DLS analysis, the average size of SeNPs was revealed to be 50–79 nm. To test the photocatalytic effects of the prepared nanoparticles, 5 mL of MB or RhB dyes (40 μM) were mixed with 20 mg of nanoparticles under UV light; 60% of MB and 75% of RhB were decomposed after 150 and 120 min,

respectively. The reaction kinetics was determined in the pseudo-first-order. Therefore, the green SeNPs showed antimycobacterial and photocatalytic good activities [60].

In 2020, a study by Britto et al. [61] investigated the effect of dye adsorption by SeNPs on RhB dye. SeNPs were produced using a leaf extract of *Justicia adhatoda* and Na_2SeO_3, and Chitosan-SeNPs were prepared with Na_2SeO_3, AA, and chitosan. The properties of Chitosan-SeNPs were determined by different analyses. The Langmuir isotherm model was used to study the adsorption of Chitosan-SeNPs. As a result, Rhodamine uptake increased with increasing concentration/temperature/under an acidic environment. The average size of Chitosan-SeNPs was 87–152 nm, and the nanoparticle size increased their reactivity, so the adsorption process was fast, then reached equilibrium within 24 h. In this case, 100 mL of Rh (20–100 mg/L) along with 1 g of absorbent material (1, 2, and 3 g/L) at pH (5.8, 6.8, and 9.4) and temperature (30, 45, and 60 °C) were used to investigate the photocatalytic effects. According to the results, photocatalytic absorption of Rh increased with the increase of nanoparticles and temperature from 30 to 60 °C. Unlike the above cases, the amount of Rh absorption should decrease with the pH increase towards basicity. When the pH is acidic, more protons are available in the reaction mixture to protonate chitosan (formation of $-NH_3^+$), resulting in an electrostatic bond between the negative charge of the dye and the positive charge of the adsorbent. The maximum adsorption limit of the Chitosan-SeNPs adsorbent was determined to be 34.5 mg/g for Rh dye [61].

The research group of Velayati [35] showed that the produced SeNPs could have photocatalytic and anticancer activity. SeNPs were synthesized using biological and green methods, including Na_2SeO_3, gum arabic (GA), and AA as a source of Se, stabilizer, and reducing agent. Synthesis of these nanoparticles was confirmed using UV–Vis, FT-IR, TEM, FE-SEM, XRD, and EDX. The UV–Vis spectroscopy outcomes exhibited a bandgap of approximately 4.85 eV for the crystalline SeNPs, corresponding to a blue shift. The EDX analysis presented the presence of distinct energy peaks at approximately 1.5 KeV, which can be attributed to the selenium metal. The XRD result showed that SeNPs had a high crystallinity and pure hexagonal phase, with an average size of about 20–24 nm. In this case, to evaluate the photocatalytic effect, 3 g of SeNPs were dissolved in 50 mL of RhB (5–10 M, pH = 9), and it was carried out for 15 to 135 min at 320 to 400 nm. SeNPs could degrade 85% RhB after 135 min in the presence of UV-A light. Based on the obtained results, the reaction kinetics was determined as pseudo-first-order [35].

In 2022, SeNPs were produced using residual-activated sludge. Residual-activated sludge is a by-product of the biological water treatment process, and 60–90 million tons of it are annually produced in countries with this industry, such as China. Activated sludge usually has high amounts of protein and carbohydrates and very low amounts of lipids. On the other hand, this prepared sludge has many uses for producing wood glue and preventing steel corrosion. In the synthesis process, polysaccharides and proteins present in residual-activated sludge were the main factors in the biological reduction of SeO_3^{2-} to SeNPs. "Domestic-wastewater activated sludge" (DWAS) and "coking-wastewater activated sludge" (CWAS) were used for the synthesis and optimization of SeNPs (DSeNPs and CSeNPs). FT-IR showed the binding of carboxyl, amine, glycoside, and other functional groups to the surface of the nanoparticles and proved that the materials in the activated sludge acted as capping agents. The nanoparticles were more stable when increasing the concentration of activated sludge, and the best pH for nanoparticle synthesis (DSeNPs and CSeNPs) was 6 and 7, respectively. The average size of CSeNPs (178.9 nm) was much smaller than DSeNPs (488.8 nm). The zeta potential of SeNPs showed that CSeNPs (-41.4 mV) were more stable than DSeNPs (-29.5 mV), which was assumed to be due to the different compounds present in the two types of activated sludge. It was found that the BET surface area of CSeNPs was much larger than DSeNPs, and on the other hand, the main shape of both types of nanoparticles was spherical. In addition, CSeNPs were able to decompose 83.94% of RhB dye after 50 min in the presence of visible light, but DSeNPs were able to decompose 78.34% of the dye after 60 min in the presence of visible light.

The corresponding reaction rate constants could reach 0.0223 (DSeNPs) and 0.0323 min^{-1} (CSeNPs) [62].

In a study in 2021, [63] Poly Anionic Cellulose (PAC), AA, and Na_2SeO_3 were used to synthesize SeNPs. UV–Vis proved the synthesis of SeNPs using PAC at 296 nm. In addition, the nanoparticles had a rod shape and crystal structure with an average particle size of 20 nm. Based on FT-IR, it was found that PAC was present around SeNPs as a capping and stabilizing agent, and their zeta potential was −43.1 mV, which indicated the high stability of these nanoparticles. In the photocatalytic investigation, it was found that 5 mg of SeNPs dissolved in RhB solution (100 mL of 5–10 M, pH = 10) decomposed 85% of the dye after 160 min under UV-A light, and the rate constant was equal to 0.0055 min^{-1}. In addition, the PAC-mediated SeNPs exhibited anticancer effects on the CT26 cell line (murine colorectal carcinoma) with an IC_{50} value of 863 µg/mL [63].

Velayati and colleagues [64] synthesized SeNPs using chitosan, AA, and Na_2SeO_3. Chitosan, as a biopolymer, can be classified as an environmentally friendly and compatible agent. The synthesis of SeNPs was initially confirmed by observing the UV–Vis absorption peak at 266 nm. The fabricated SeNPs had a rod-shaped structure with an average size of 20–27 nm. The XRD pattern showed high crystallinity and a pure hexagonal phase. Based on FT-IR results, the produced nanoparticles were capped by chitosan and amine groups. The prepared SeNPs had negatively charged groups in their structure, which was detected by zeta potential (−35.46 mV). The bandgap energy of the SeNPs product was observed to be 4.30 eV, which is reasonably higher in comparison to its bulk state of 2.0 eV. In the photocatalytic evaluation, 5 mg of SeNPs was added to 100 mL of RhB solution (6–10 M and pH = 10) under a UV light source, which was able to decompose 85% of the dye after 120 min. In addition, SeNPs exhibited anticancer effects on CT-26 and HT-29 cell lines with IC_{50} values of 750 and 500 µg/mL, respectively [64].

2.3. Bromothymol Blue

Bromothymol blue (BTB) is a pH indicator often used to identify the presence of carbonic acid in a liquid and as an indicator in packaging materials. In addition, it is used to check the activity of the fungal asparaginase enzyme, observe photosynthetic activities, differentiate between the nucleus and the cell wall in the laboratory, and check the premature rupture of the membranes in gynecology and obstetrics. It acts as a weak acid in the solution and can be protonated or deprotonated, and the color of the solution changes from yellow to blue. The maximum UV–Vis absorption peak of the protonated and deprotonated form of this compound is observed at the wavelength of 427 and 602 nm, respectively. Exposure to this substance can cause irritation and inflammation of the skin, eyes, and respiratory tract [65,66].

The study published by Ameri et al. [32] aimed to synthesize SeNPs using selenium dioxide (SeO_2, selenium sources) and *Streptomyces griseobrunneus*. The average size of prepared NPs was 73.8 nm with a spherical shape. The FT-IR spectrum of the produced nanostructures did not display any distinctive or pronounced absorption band associated with the functional groups present on the surface of the biogenic SeNPs. The corresponding XRD pattern of the purified biogenic SeNPs provided evidence of the creation of trigonal Se. After that, the reaction mixture required for the photocatalytic test includes BTB (180 µg/mL) dissolved in 50 mM citrate buffer (pH = 5) and SeNPs (4–64 µg/mL), which was investigated in 10–60 min at 254 nm (15 W UV lamps). The result showed 64 µg/mL of SeNPs removed 62.3% of BTB under UV after 60 min incubation. The degradation rate of BTB was 32.5% using SeO_2 (64 µg/mL) after the same time [32].

2.4. Malachite Green

Malachite green (MG) is a triphenylmethane cationic dye soluble in water. The maximum UV–Vis absorption of this dye is observed in the range of 618 nm. Due to its cheapness and availability, it is widely used in aquaculture industries all over the world to treat protozoan and fungal infections in aquatic animals. It can also reduce the photosynthesis of algae

by preventing light from entering the water and ultimately reduce the life quality of aquatic animals [67,68]. On the other hand, MG is stable in the environment, like other dyes. Its consumption can cause eye burns; rapid breathing; damage to the nervous system, brain, and liver; lesions on the skin and lungs; etc. Most importantly, this dye can cause cancer in different parts of the body and teratogenicity. For all these reasons, the "World Food and Drug Organization" has announced MG as an oleate-containing chemical substance to investigate carcinogenesis and provide a solution to prevent human poisoning by this dye [67,68].

In 2023, the green synthesis of SeNPs was performed using pure *Aspergillus tereus* cells by the research team of Saied [69] in an environmentally friendly and green method. Na_2SeO_3 was used as a precursor for the production of SeNPs. TEM analysis showed the spherical SeNPs with size of 10–100 nm. The XRD pattern of SeNPs prepared by A. terreus confirmed the crystalline phase of Se (a monoclinic structure of SeNPs). The reaction mixture required for the photocatalytic test on MG includes 100 mL of MG (100 μg/mL) and different concentrations of SeNPs (0.25, 0.5, 0.75, and 1 mg/mL) in a period of 30–300 min at 624 nm under sunlight. The results showed that 1.0 mg/mL SeNPs decompose 89% of GM after 240 min. In addition, the prepared nanoparticles displayed strong antibacterial and weak antifungal effects in addition to decolorizing properties [69].

2.5. Sunset Yellow Azo

Sunset Yellow FCF azo-dye (SY) is one of the most common dyes in the food industry and is widely used in cereals, candies, dairy products, yogurt, soft drinks, ice creams, chocolate, etc. Consumption of SY may cause allergic reactions, worsen asthma symptoms, digestive problems, possibly ADHA in children, tumors, cancer, liver toxicity, and kidney failure. Like other azo dyes, SY is resistant to light, heat, and biodegradation due to the presence of the azo group and aromatic rings. SY exhibits λmax at about 480 and 443 nm at pH = 1 and 13, respectively [70–72].

Hassanin and colleagues, in 2019, [73] were able to synthesize green SeNPS using *Moringa olifera* extract and Na_2SeO_3. The XRD pattern proved the crystalline SeNPs with an average size of 18.85 nm. SEM and TEM indicated the spherical shape of the green SeNPs with a range of 23–35 nm. The measured value for the optical bandgap of the direct transition was found to be 2.3 eV. It was observed that the SeNPs synthesized through green methods possess a bandgap energy that is greater than that of the bulk α-Se (2.0 eV) and commercial Se powder (1.8 eV) due to the quantum size effect. SeNPs had the capability of degrading SY dye under both UV and solar irradiations. The reaction conditions included SY (5 mg/mL) and SeNPs (0.3 g/L) at pH = 5.8; the degradation rates of the dye for sunlight and UV radiation after 10 h were 83.8 and 76.6%, respectively. The photocatalytic reaction was pseudo-first-order kinetics, and the rate constant was determined to be 0.173 min^{-1} [73].

2.6. Fuchsin

Basic Fuchsin dye is a cationic dye belonging to triarylmethane dyes. It is flammable and is used in dyeing textiles, leather, cotton, silk fibers, tissues, and organs. In addition, this dye has bactericidal, fungicidal, and anesthetic properties. Fuchsin, like the other dyes mentioned, has high stability and is non-biodegradable. In addition, it can cause cancer and irritation of the digestive system and the respiratory tract. Due to these factors, the entry of Fuchsin into the water–sewage system leads to environmental pollution, which is a matter of great concern. Therefore, it is imperative that we find a solution to this problem [74–76].

Badreah et al., in 2020, ref. [77] synthesized SeNPs in the presence of AA and polyvinyl alcohol; the nanoparticles were semi-spherical with a diameter of 8–22.5 nm. In the aggregated sphere, the diameter of the SeNPs was determined to be 470–710 nm. XRD confirmed the presence of SeNPs in a crystalline form and also showed their high purity after preparation. In the photocatalytic degradation studies, after 20 min from the irradiation time, only 70.9% of the substance was decomposed when 5 mg of SeNPs was utilized. However, as the

dosage of SeNPs increased, the degradation efficiency significantly improved, ultimately reaching 96.4% within 40 min. Changes in the concentration of SeNPs were studied to investigate the complete removal of Fuchsin dye from aqueous solution. Continuing with this approach, by elevating the dosage to 10 mg, the complete degradation of Fuchsin was achieved within a mere 34 min under visible light irradiation. All the systems conform to the pseudo-first-order kinetic principle while containing a significant amount of SeNPs. The use of green synthesis methods for producing SeNPs increases the efficiency of radicals ($^\circ$OH), which is the main factor necessary for the photocatalytic effect to remove contaminants [77].

2.7. Congo Red, Methyl Orange, and Safranine T

Congo red (CR) is one of the synthetic and azo (N=N) dyes. The maximum UV–Vis absorption peak of CR is observed at 497 nm. CR is used in the textile, paper, dye, and cosmetic industries. In addition, this dye has an azo group, aromatic structure, high stability, and high solubility in water. On the other hand, CR is carcinogenic and remains in the environment for a long time, so it negatively affects plants and animals. The use of CR has been banned in some countries due to its side effects and toxicity, but it is commonly used in many other countries. Therefore, it is necessary to treat water contaminated with CR [78,79].

Safranin T (ST), as a basic dye, is an important and traditional phenazinium dye. ST is an azine dye that is widely used and belongs to the category of synthetic dyes that have existed for a long time [80,81]. The ST dye has been extensively utilized in academic research as a tool for spectroscopic analysis and as an indicator. It possesses a planar structure and cationic charge. It has the ability to easily be inserted into large biological molecules, such as DNA and proteins [82]. ST is a powder that dissolves in water and has a reddish-brown color [81].

Methyl orange (MO) is an anionic azo dye (sulphonated azo group). MO (orange-yellow powder with melting point >300 °C) is partially soluble in normal water, highly soluble in hot water, and insoluble in ethanol. MO can act as a weak acid in water (pH ~6.5). MO, as a pH indicator, shows a red color in the acidic condition and an orange color in the basic condition. The high chemical stability, intense coloration, toxicity, and low biodegradability of MO can be attributed to its azo group, sulfur group, and aromaticity [83].

In 2018, Xia and colleagues [36] used "*Escherichia coli* strain S17-1 pCT-Zori-csrF" and Na_2SeO_3 to produce bio-SeNPs. According to the results of systematic analysis (TEM, SEM, and DLS) of bio-SeNPs, it was found that they had irregular spheres with a diameter of 60–105 nm. The Zeta potential exhibited a positive charge at low pH values ($\leq$6) and a negative charge at high pH values ($\geq$7). As the pH value increased, the Zeta potential gradually decreased. The effect of dye removal on three dyes of CR, ST, and MB showed that the highest adsorption was for anionic dye (CR) at acidic pH and cationic dye (ST and MB) at alkaline pH. In this case, the synthesized SeNPs (0.4 g/L) were incubated with the desired dyes (200 mg/L; CR, ST, and MB) separately in the range of pH = 5–10. The absorption wavelength investigated in this case for CR, ST, and MB were 437, 520, and 660 nm, respectively. According to the results, with increasing pH, the removal efficiency of CR decreased, but with increasing pH, the removal efficiency of ST and MB increased. The obtained results, together with the zeta potential data, exhibited that at low pH, the synthesized nanoparticles have a positive charge, and they can give stronger absorption with anionic dyes (CR) and increase the photocatalytic effect related to CR. On the other hand, the synthesized nanoparticles have a negative charge and give stronger absorption with cationic dyes (ST and MB) at a high pH. Therefore, the optimum pH for checking the photocatalytic effect of CR, ST, and MB was 5, 10, and 10, respectively. MB needed only 5 min to display the total absorption while CR and ST needed 35 and 25 min, respectively. Dye removal efficiency increased with increasing temperature. The adsorption capacities of bio-SeNPs for CR, ST, and MB were determined to be 1577.7, 1911.0, and 1792.2 mg/g, respectively, which were 6.8, 25.2, and 49.0% higher than that for other bio-based materials,

respectively. The pseudo-second-order model is suitable for the adsorption kinetics of Bio-SeNPs for CR, ST, and MB. It is an important advantage to note that the fabricated nanoparticles can be reused with 200 mM NaCl even after five times of dye removal [36].

Ahluwalia et al. [84] biosynthesized SeNPs as a cocatalyst using *Bacillus* sp. and Na_2SeO_3 to improve the photocatalytic activity of ZnS for the decomposition of MO dye under UV light. SEM analyses of SeNPs showed a diameter range of 50–200 nm with a spherical shape and smooth surface. SeNPs with varying weight percentages were utilized in the impregnation process onto ZnS through calcination at 200 °C to yield SeZnS nanocomposites. The XRD pattern of ZnSNPs was perfectly indexed to the cubic phase of ZnS while the XRD of the Se-ZnSNCs matched with a hexagonal selenium phase. The TEM micrograph revealed that the ZnSNPs form clusters of particles with a rough surface, exhibiting sponge-like and porous structures with an average size of 40–80 nm. In the degradation process, 1 wt% SeZnS nanocomposites displayed 95% MO degradation in comparison to ZnS, which showed only 55% degradation under 160 min of UV light exposure. It should be noted that the reaction adhered to pseudo-first-order kinetics, with an impressive rate constant of 0.00842 min^{-1} [84].

Generally, according to the reviewed articles, various precursors, such as Na_2SeO_3, $HSeO_3$, and Se powder, were used for the synthesis of green SeNPs; most of them used Na_2SeO_3 salt during the synthetic process. In addition, plant extracts, biological media (bacteria, fungi, etc.), and environmentally compatible compounds (ascorbic acid, gelatin, glucose, starch, etc.) were employed as reducing, stabilizing, and caping agents in the production of green SeNPs. On the other hand, various studies have shown that these green synthesized SeNPs, in addition to the significant biological effects in various fields, had the catalytic ability to reduce or decompose different dyes under various irradiations, the most reports of which were about the reduction or decomposition of MB and RhB dyes. The photocatalytic activity of Se is related to the electronic bandgap properties that make it a compelling candidate for photonic and catalytic applications, where efficient charge separation and reaction initiation are critical. The electronic bandgap characteristics of Se and its implications for photocatalysis in comparison to other metals and semiconductors are as follows: the narrower bandgap of Se is advantageous for efficient photon absorption, promoting enhanced photoexcitation, and improved electron–hole separation. The bandgap values of Ag, Au, TiO_2, ZnO, etc., are larger than that of Se, leading to a reduced likelihood of photon-to-electron–hole conversion in photocatalytic processes. Consequently, the efficiency of these metals as a photocatalyst may be lower compared to Se. Therefore, based on bandgap characteristics, Ag, Au, etc., are likely less suitable for photocatalysis compared to Se. In other words, materials with smaller bandgaps generally exhibit superior performance in photocatalysis [85,86].

Table 1. Some essential information about the reported SeNPs and their catalytic activities.

NPs	Biosources	Salts	Size (nm)	Shape	Dyes	Irradiations		Ref
SeNPs	Yeast	Na_2SeO_4	170–240	Rod	MB	Visible	-	[34]
SeNPs	*W. somnifera*	H_2SeO_3	45–90	Spherical	MB	Sunlight	-	[43]
Se nanowires	Sodium formaldehyde sulfoxylate	SeO_2	100–200	Rod	MB	Visible	H_2O_2	[44]
SeNPs	*F. benghalensis*	Se powder, sodium sulphide	45–95	Spherical	MB	UV	-	[45]
SeNPs	*M. purpureus*	Na_2SeO_3	46.58	Round	MB	Sunlight	-	[46]
SeNPs	Glucose, AA, starch	Na_2SeO_3	2–10	Spherical	MB	UV	-	[47]
SeNPs	*C. bulbosa* tuber	H_2SeO_3	55.9	Spherical	MB	Halogen lamp	-	[48]
SeNPs	*G. wightii*, AA	Na_2SeO_3	80	Spherical	MB	Sunlight	-	[37]
SeNPs	*A. paradoxum*	Na_2SeO_3	37.5	Semi-spherical	MB	-	$NaBH_4$	[49]
SeNPs	*C. caspius*	Na_2SeO_3	20.34	Spherical	MB	-	$NaBH_4$	[50]
SeNPs	*H. esculentus*	Na_2SeO_3	62	Spherical	MB	-	$NaBH_4$	[51]
SeNPs	Sulfite reductase in *Lysinibacillus* sp. ZYM-1	Na_2SeO_3	100–200	Cubic and spherical	RhB	Visible	H_2O_2	[59]
SeNPs	Gelatin, AA	Na_2SeO_3	<20	Spherical	RhB, MB	UV	-	[60]
Chitosan-SeNPs	*J. adhatoda*	Na_2SeO_3	87–152	-	RhB	-	-	[61]
SeNPs	GA, AA	Na_2SeO_3	20–24	-	RhB	UV-A	-	[35]
SeNPs	sludge	SeO_3^{2-}	178.9, 488.8	Spherical	RhB	Visible	-	[62]
PAC-Se nanorods	PAC, AA	Na_2SeO_3	20	Rod	RhB	UV-A	-	[63]

Table 1. *Cont.*

NPs	Biosources	Salts	Size (nm)	Shape	Dyes	Irradiations		Ref
Se nanorods	Chitosan, AA	Na_2SeO_3	20–27	Rod	RhB	UV	-	[64]
SeNPs	*S. griseobrunneus*	SeO_2	73.8	spherical	BTB	UV	H_2O_2	[32]
SeNPs	*A. tereus*	Na_2SeO_3	10–100	Spherical	MG	Sunlight	-	[69]
SeNPs	*M. olifera*	Na_2SeO_3	23–35	Spherical	SY	UV, solar	-	[73]
SeNPs	AA, polyvinyl alcohol	Na_2SeO_3	8–22.5	Semi-spherical	Fuchsin	Visible	-	[77]
SeNPs	*E. coli*	Na_2SeO_3	60–105	Irregular spheres	CR, ST, MB	-	-	[36]
Se-ZnS nanocomposites	*Bacillus* sp., calcination	Na_2SeO_3, $ZnNO_3$, L-cysteine	-	Cluster form	MO	UV	-	[84]
NiSeNPs	*H. rosa-sinensis*	$NiCl_3$, Se powder	26	Spherical	MB	Visible	-	[52]
Cu_2Se sheets	AA, β-CD	Se powder, $Cu(CH_3COO)_2$	-	Sheet	MB	Visible	H_2O_2	[53]
Cu_2Se_3, Cu_2Se_3/rGO	Gly, $NaBH_4$, GO	Se powder, $Cu(NO_3)_2$	75, 25	Dendritic-like	MB	Solar/visible	-	[54]
CuxSey/PANI	Gly, $NaBH_4$	Se powder, $Cu(NO_3)_2$, PANI	25	-	MB	Visible	-	[55]

In order to enhance the photocatalytic activity of metals characterized by wide bandgaps and limited photocatalytic efficiency, four prominent approaches are frequently employed: metal/nonmetal doping/co-doping, semiconductor coupling, coupling with carbon materials, and dye sensitization. These methods are utilized to address the challenge of poor performance exhibited by materials with large bandgaps. Through techniques the goal is to optimize and promote photon absorption, charge separation, and overall photocatalytic performance within the visible light spectrum. These strategies aim to harness the untapped potential of materials with wide bandgaps and thereby elevate their effectiveness in photocatalytic applications [87–93]. For example, in a study (2017) [90], tetra (4-carboxyphenyl) porphyrin (TP) compound, as a visible antenna, was used to improve the photocatalytic effects of TiO_2. It was found that the bandgap energy of TiO_2 was 2.95 eV, which was reduced to 2.6 eV by adding TP part and synthesizing TP-TiO_2. Finally, TP-TiO_2 can degrade about 93% of RB after 10 h using visible irradiation [90]. In another study, quinazoline derivative (Q) as a semiconductor was utilized to improve the photocatalytic activity of TiO_2. The evaluated bandgap energy of TiO_2 NPs was 2.97 ± 0.05 eV, which decreased to 2.58 ± 0.05 eV after merging with compound Q. Next, RhB removal after 3 h under visible and UV-A irradiations was 82% and 98%, respectively, while TiO_2 NPs degraded 93% of RhB after 5 h [85]. Another way to increase the photocatalytic activity of NPs that have a large bandgap is to use polymers (CP) that are coordinated to the target metal. In 2017, bis(imidazole) derivatives as N-donor CPs were used to increase the photocatalytic activity of Co (II). The photodegradation rate of MB increased (after 120 min) to 91.4% and 89.1% in the presence of two bis(imidazole) derivatives while these compounds approximately are not able to degrade MB under dark and normal conditions [94]. In another study, 2,4,6-tris(4-pyridyl)-1,3,5-triazine (tpt) as an O-donor ligand was employed to enhance the photocatalytic properties of Zn (II). The results of the photocatalytic investigation on MB revealed that Zn-tpt could achieve an 89% degradation of the MB under illumination after 4 h [95].

3. Mechanism of Photocatalytic Activity of SeNPs (Figures 2–11)

Generally, in the photocatalytic degradation of different dyes, when light radiates to the solution containing SeNPs-dye, its energy is absorbed by SeNPs (Figure 11). As a result of this energy absorption, an electron (e^-) moves from the valence band (VB) to the conduction band (CB), and at the same time, holes (h^+) in the band capacity are created to reduce or oxidize organic substances. Both e^- and h^+ generated contribute to the photocatalytic process. The holes created in the valence band have a strong oxidizing ability, and if it is in a humid environment (H_2O), it can absorb moisture and produce hydroxyl radicals ($OH^°$). Electrons (e^-) transferred to the valence layer using O_2 in the environment can produce superoxide anion radicals ($^°O_2{}^-$). In addition, if H_2O_2 is used in the photocatalytic process, it can produce hydroxyl radical ($OH^°$) with the help of H_2O_2. The produced superoxide anions also eventually become hydroxyl radicals ($OH^°$). Finally, due to their high oxidizing ability, hydroxyl radicals ($OH^°$) react with organic substances

(dyes) absorbed on the surface of nanoparticles, and colored pollutants become non-toxic products (Figures 2–10), and finally, these compounds are decomposed to components associated with minerals, such as CO_2, H_2O, $SO4^{-2}$, NO_3^-, etc. [44,64,96].

MB has a strong blue dye due to the transfer of its electron to the π between N and S atoms. On the other hand, due to this electron transfer, a UV absorption peak is observed in the region of 665 nm. Another UV peak of this compound is observed in the region of 615 nm, which is related to electron transfer in the conjugated aromatic structure. Research has shown that the extract encapsulated around nanoparticles acts as a catalyst for oxidation–reduction reactions in the photocatalytic process. Due to the reduction in the central part of MB during the catalytic process, electron conjugation in the structure and electron transfer between N and S is lost, a colorless structure is formed, and a shift occurs in the absorption peaks of 664 and 615 nm. In the first step, hydroxyl radicals attack the functional group $C-S^+=C$ in MB, turn this part into $C-S(=O)-C$, and also cause the opening of the aromatic ring containing both N and S heteroatoms (Figure 2). In the next steps, the aromatic rings are separated, and N-de-methylation occurs. After complete degradation, finally, the color of the solution containing MB will change from blue to colorless, and the main product of this degradation will be CO_2 and H_2O [97,98].
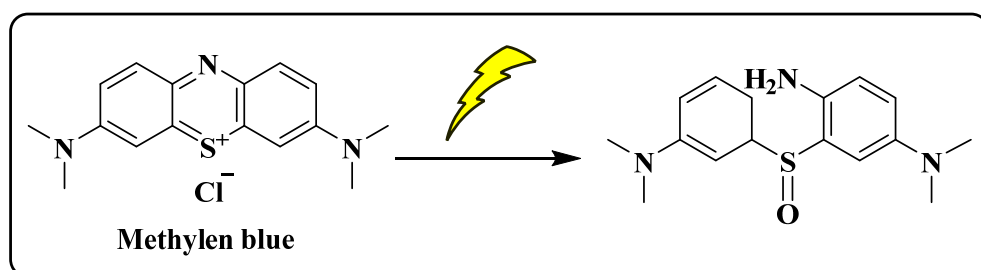
Figure 2. The photodegradation derivative of Methylene blue.

In another photocatalytic mechanism in the presence of sodium borohydride, nanoparticles (catalytic surface) act as both "electron donors and acceptors", facilitating the transfer of electrons in a redox reaction and ultimately moving H^- on the surface of the dye. For the reduction of dye using nanoparticles, BH_4^- is adsorbed onto the nanoparticles, and the self-hydrolysis of BH_4^- results in the production of BO_2^-. The formation of "active surface-hydrogen" (H^-) occurs in a temporary manner through the transfer of "active hydrogen species" from BH_4^- to the nanoparticles. Subsequently, the dye is reversibly attached to the surface of the nanoparticles. At the same time, "the active surface hydrogen" is transferred to the dye and produces the related reduced compound. Actually, the nanoparticles assist in transferring electrons from BH_4^- to MB and RhB dyes, resulting in the formation of colorless substances, namely leuko MB and leuko RhB (Figure 3). A similar reaction for ST can occur and create a colorless derivative (Figure 3). The completion of the catalytic reduction of the dyes is indicated by the achievement of the baseline absorption intensity of dyes [99–101]. This reduction mechanism can also be considered for azo dye, which the azo group reduced during the reduction process, such as SY (Figure 8), MO (Figure 9), and CR (Figure 10) [100].

Different studies found that the degradation process of RhB (Figure 4) can proceed in two ways. In the first case, N-de-ethylation occurs when the aromatic structure is stable, but the color of the solution containing RhB-SeNPs does not change. The second step is the removal of the acid group of benzoic acid, and this group is considered an RhB chromophore group. In this step, the molecular conjugation system is destroyed, and the color of the solution changes to pale and colorless. In the continuation of the degradation path, the rings in the xanthene structure (that was left over from the second stage) are opened, and the aromatic system is destroyed. Finally, all the structures are converted into CO_2 and H_2O, and the intensity of the UV–Vis absorption peak decreases in the region of 554 nm [102–104].

In addition, the pH level of the solution has an impact on the photocatalytic ability. Ayoub and coworkers exhibited that the BTB solution (as shown in Figure 5) is able to almost completely degrade during 70 min when exposed to UV light in a basic medium (pH = 10). The duration of this process is longer in the acidic environment. The efficiency of OH radicals in degrading organic molecules is significantly influenced by the structure of the molecule. Furthermore, a variation in pH affects the photodegradation of azo dyes (Figures 8–10) and can cause their degradation [105,106]. In the degradation process, other structural changes of different dyes (Figures 6–10) included N-de-alkylation (MG), breaking or reduction of the azo bond (SY, MO, CR), and de-amination. Then, the aromatic structure is destroyed, and finally, the existing structures become CO_2 and H_2O, and the toxicity and color of the compounds are removed [107–111].
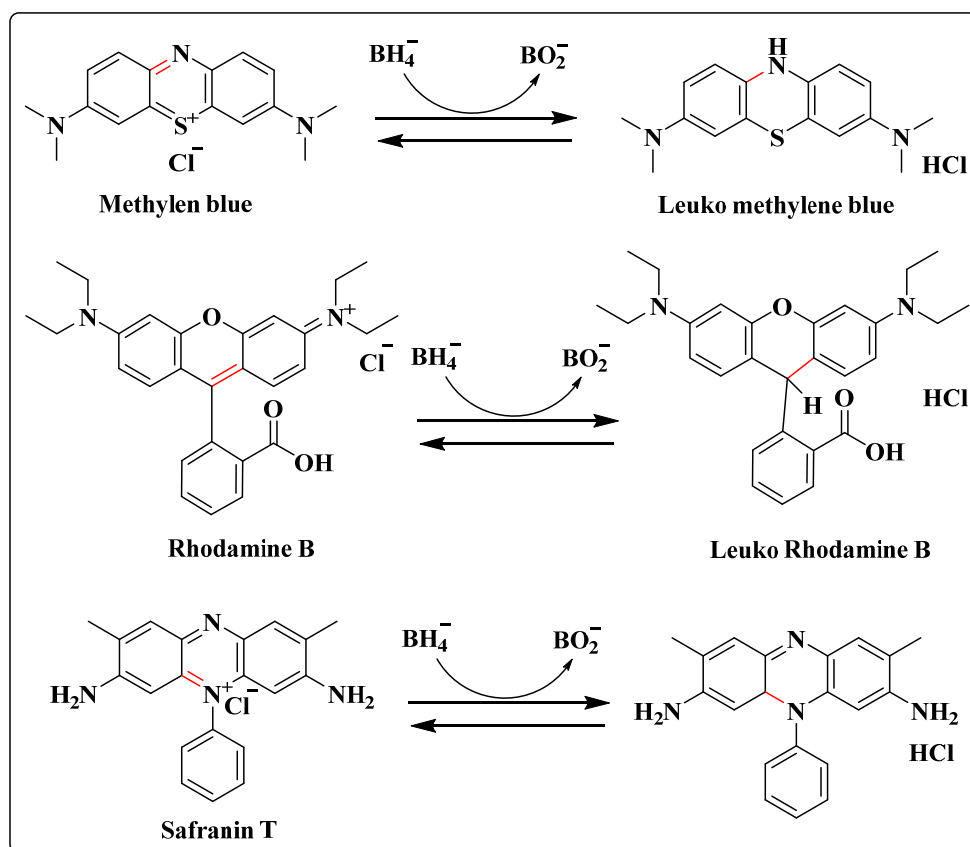
Figure 3. The reduction of MB, RhB, and ST.
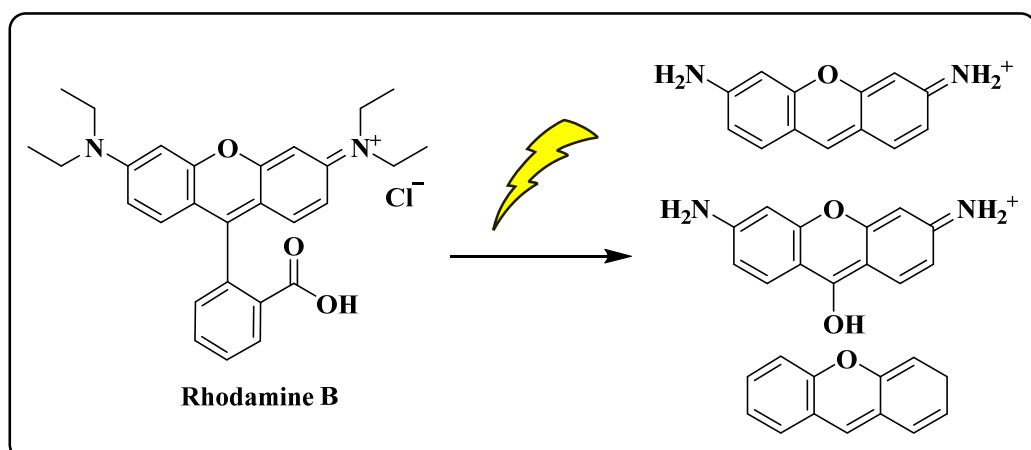
Figure 4. The photodegradation derivative of Rhodamine B.
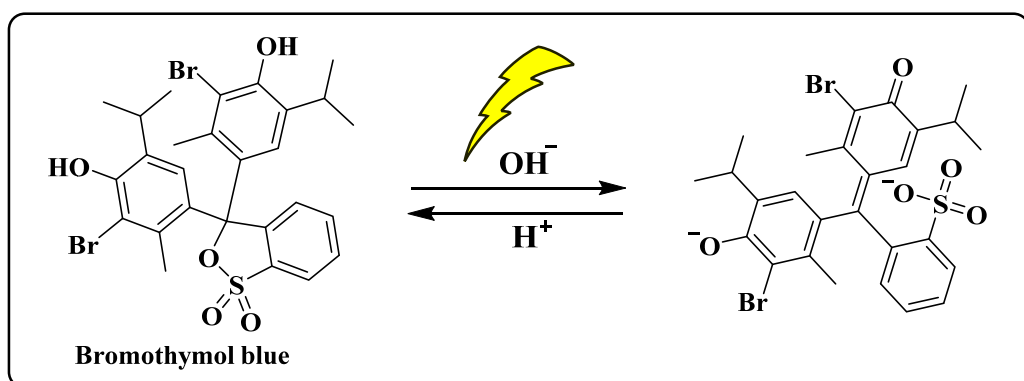
Figure 5. The photodegradation derivative of Bromothymol Blue.
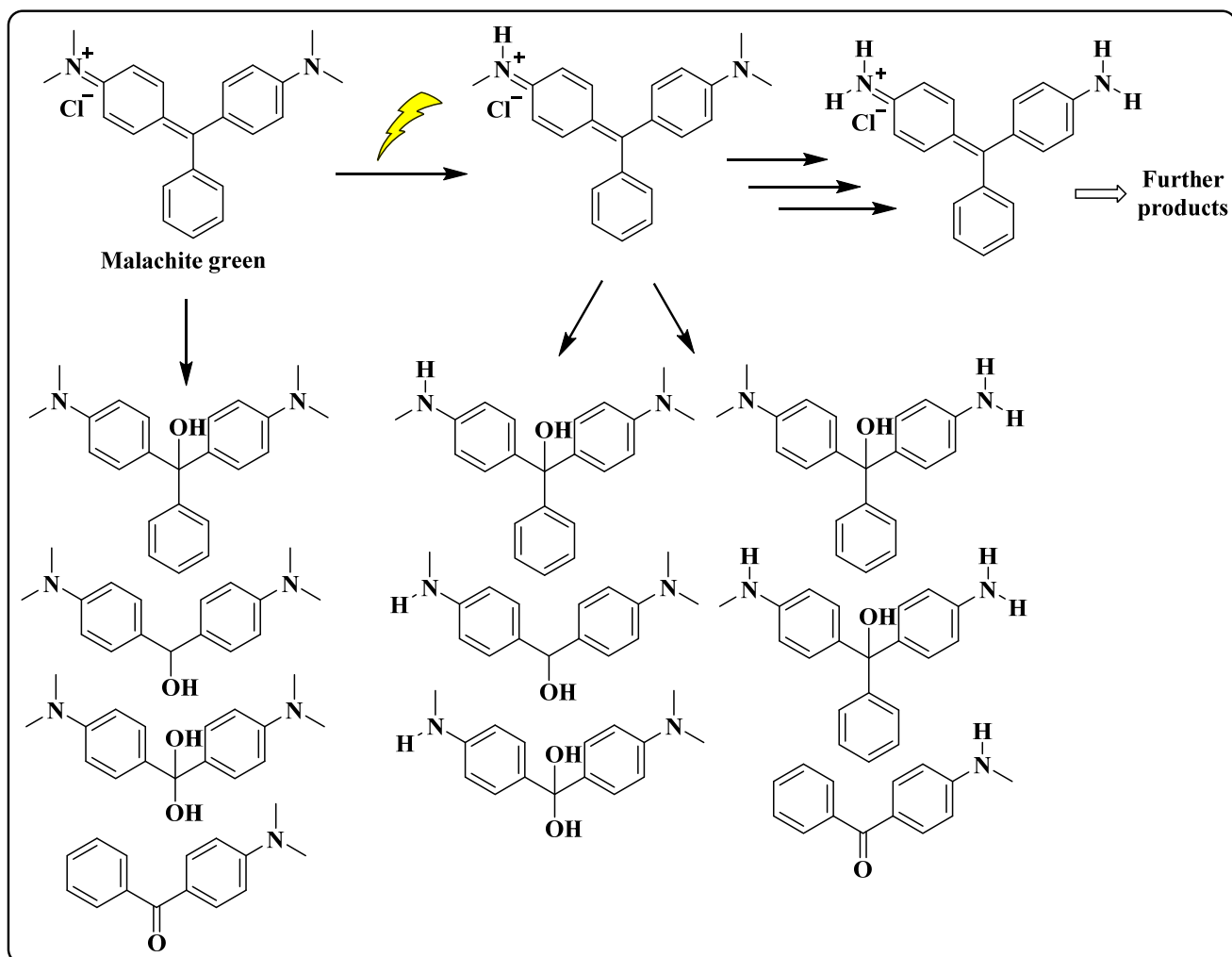
**Figure 6.** The photodegradation derivatives of Malachite green.
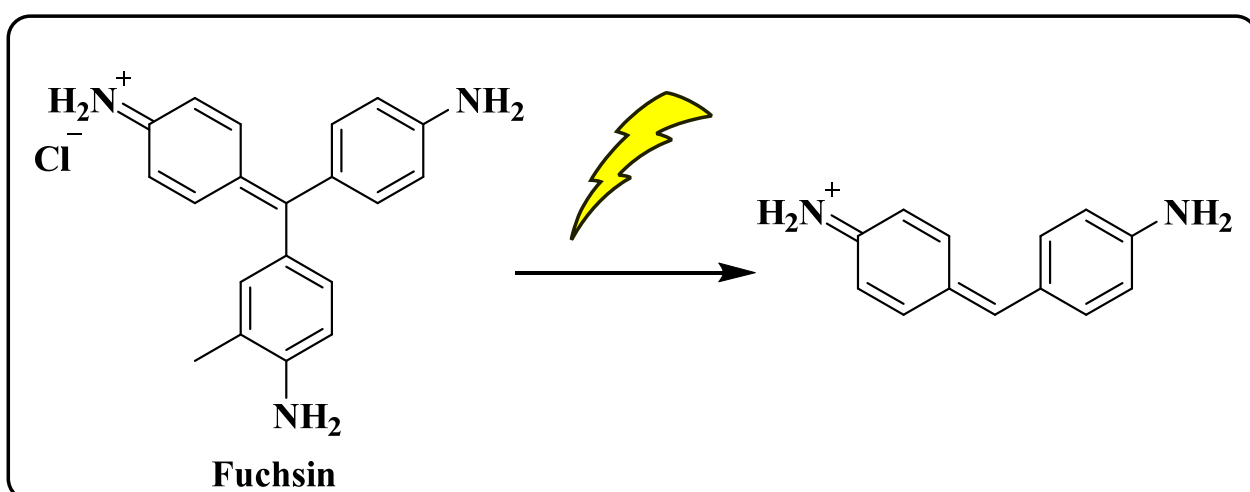
**Figure 7.** The photodegradation derivative of Fuchsin.
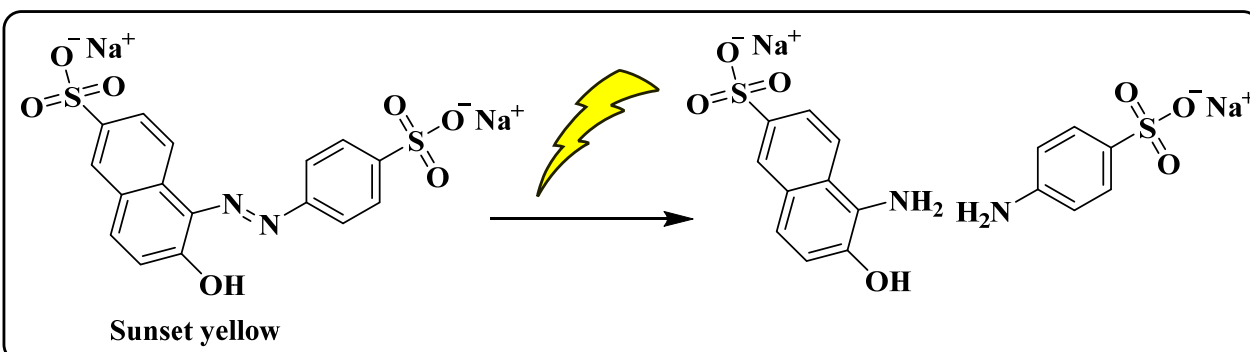
**Figure 8.** The photodegradation derivatives of Sunset Yellow Azo.
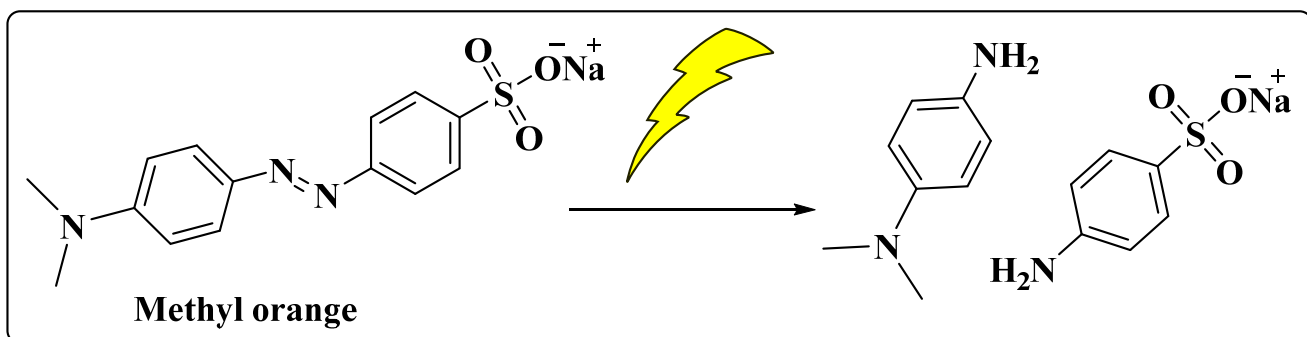
**Figure 9.** The photodegradation derivatives of Methyl orange.
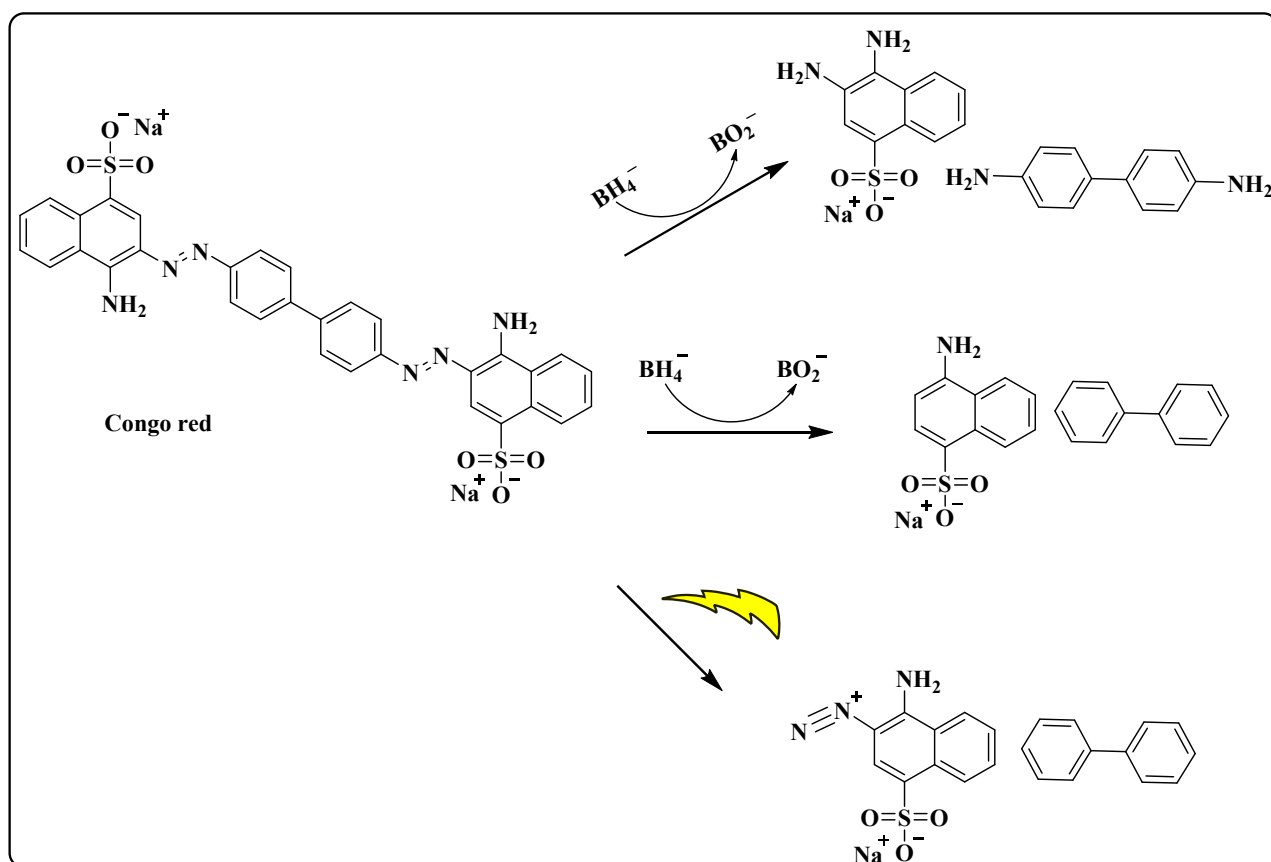
**Figure 10.** The photodegradation derivatives of Congo Red [100].
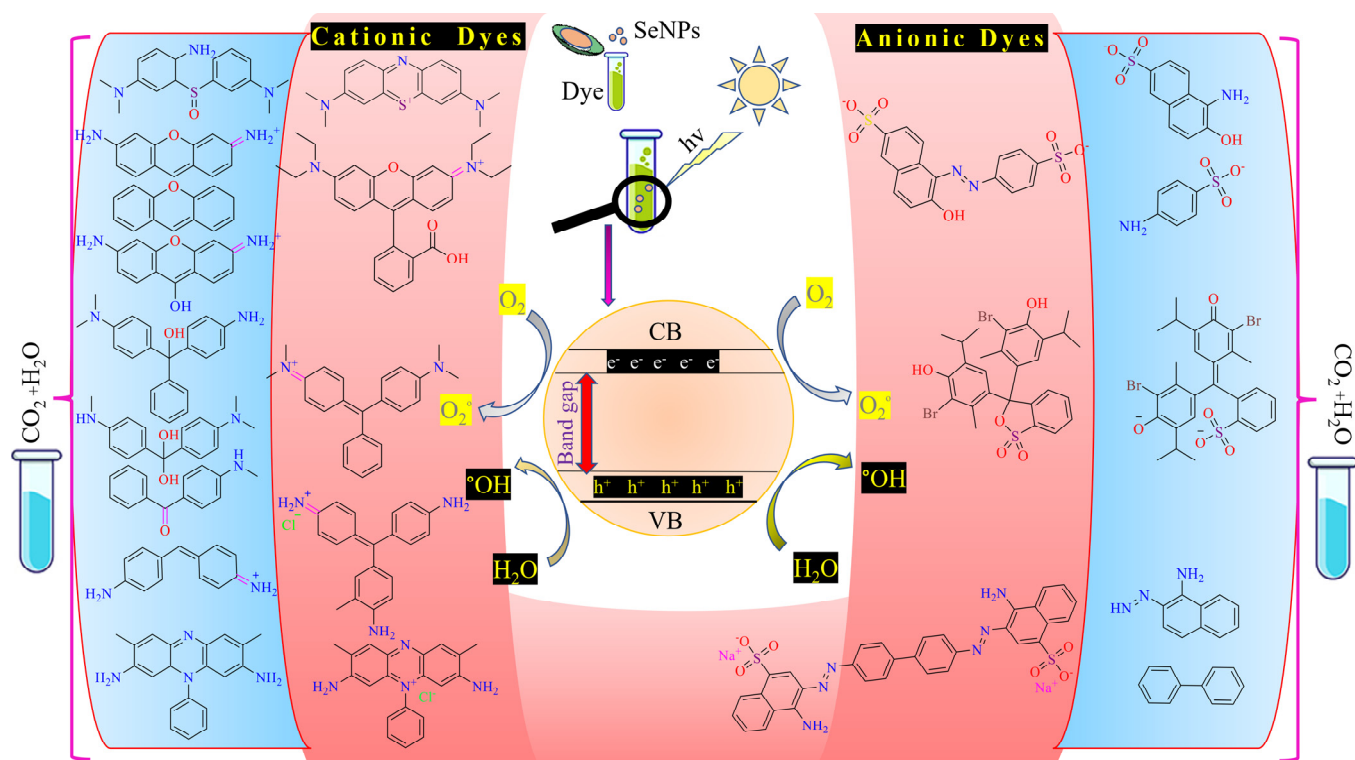
Figure 11. Degradation process of several dyes.

4. Conclusions

In recent years, special attention has been paid to the synthetic method of nanoparticles using plant extracts or microorganisms. The green method is cost-effective, safe, renewable, and non-toxic. Due to tunable surface plasmon resonance and high surface areas, these nanoparticles have special applications, particularly as catalysts in removing dyes from wastewater. SeNPs possess various exceptional biomedical characteristics and exhibit superior biocompatibility and degradability compared to alternative metal nanoparticles. Due to the increase in the industrialization of countries, the amount of pollutants entering water and wastewater has increased a lot. Water containing pollutants and dyes causes fatal diseases in humans and is dangerous for aquatic animals. There are different methods (physical, chemical, etc.) to remove organic dyes from water and wastewater. One of the best ways is the use of green SeNPs for the catalytic decomposition of water pollutants (dyes), in which the pollutants are converted into harmless byproducts. SeNPs, with their special characteristics, can cause structural changes in dyes (reduction of N=N, C=N or C=C bonds, N-de-alkylation, etc.) due to the production of $^{\circ}O_2{}^{-}$ and OH° under UV light irradiation. Finally, the conjugated structure of the dye is destroyed (transformation of the degradation structure into CO_2 and H_2O), eliminating or reducing the toxicity of the dyes. By reviewing the significant developments in this field, this comprehensive review can potentially present new prospects for creating and assembling exceptionally efficient green SeNPs-based photocatalysts that can be applied in various photocatalytic processes.

References

1. Mekonnen, T.B. An overview on the photocatalytic degradation of organic pollutants in the presence of cerium oxide (ceo 2) based nanoparticles: A review. *Nanosci. Nanometrol.* **2021**, *7*, 14–26. [CrossRef]
2. Gusain, R.; Gupta, K.; Joshi, P.; Khatri, O.P. Adsorptive removal and photocatalytic degradation of organic pollutants using metal oxides and their composites: A comprehensive review. *Adv. Colloid Interface Sci.* **2019**, *272*, 102009. [CrossRef] [PubMed]
3. Weldegebrieal, G.K. Synthesis method, antibacterial and photocatalytic activity of ZnO nanoparticles for azo dyes in wastewater treatment: A review. *Inorg. Chem. Commun.* **2020**, *120*, 108140. [CrossRef]
4. Su, R.; Dai, X.; Wang, H.; Wang, Z.; Li, Z.; Chen, Y.; Luo, Y.; Ouyang, D. Metronidazole degradation by UV and UV/H_2O_2 advanced oxidation processes: Kinetics, mechanisms, and effects of natural water matrices. *Int. J. Environ. Res. Public Health* **2022**, *19*, 12354. [CrossRef] [PubMed]
5. Isa, E.D.M.; Shameli, K.; Jusoh, N.W.C.; Sukri, S.N.A.M.; Ismail, N. Photocatalytic degradation with green synthesized metal oxide nanoparticles—A mini review. *J. Nanosci. Nanotechnol.* **2021**, *2*, 70–81.
6. Marimuthu, S.; Antonisamy, A.J.; Malayandi, S.; Rajendran, K.; Tsai, P.-C.; Pugazhendhi, A.; Ponnusamy, V.K. Silver nanoparticles in dye effluent treatment: A review on synthesis, treatment methods, mechanisms, photocatalytic degradation, toxic effects and mitigation of toxicity. *J. Photochem. Photobiol. B Biol.* **2020**, *205*, 111823. [CrossRef]
7. Pandey, A.; Shukla, P.; Srivastava, P.K. Remediation of dyes in water using green synthesized nanoparticles (NPs). *Int. J. Plant Env.* **2020**, *6*, 68–84. [CrossRef]
8. Vedhantham, K.; Girigoswami, A.; Harini, A.; Girigoswami, K. Waste water remediation using nanotechnology—A review. *Biointerface Res. Appl. Chem.* **2022**, *12*, 4476–4495.
9. Akbari, A.; Sabouri, Z.; Hosseini, H.A.; Hashemzadeh, A.; Khatami, M.; Darroudi, M. Effect of nickel oxide nanoparticles as a photocatalyst in dyes degradation and evaluation of effective parameters in their removal from aqueous environments. *Inorg. Chem. Commun.* **2020**, *115*, 107867. [CrossRef]
10. Anandan, S.; Vinu, A.; Mori, T.; Gokulakrishnan, N.; Srinivasu, P.; Murugesan, V.; Ariga, K. Photocatalytic degradation of 2,4,6-trichlorophenol using lanthanum doped ZnO in aqueous suspension. *Catal. Commun.* **2007**, *8*, 1377–1382. [CrossRef]
11. He, Y.; Sang, W.; Lu, W.; Zhang, W.; Zhan, C.; Jia, D. Recent advances of emerging organic pollutants degradation in environment by non-thermal plasma technology: A Review. *Water* **2022**, *14*, 1351. [CrossRef]

12. Feiona, T.A.; Sabeena, G.; Bagavathy, M.S.; Pushpalaksmi, E.; Jenson Samraj, J.; Annadurai, G. Recent advances in the synthesis and characterization of nanoparticles: A green adeptness for photocatalytic and antibacterial activity. *Nat. Environ. Pollut. Technol.* **2021**, *20*, 657–663. [CrossRef]

13. Raza, M.A.; Kanwal, Z.; Rauf, A.; Sabri, A.N.; Riaz, S.; Naseem, S. Size-and shape-dependent antibacterial studies of silver nanoparticles synthesized by wet chemical routes. *Nanomaterials* **2016**, *6*, 74. [CrossRef] [PubMed]

14. Danish, M.S.S.; Estrella-Pajulas, L.L.; Alemaida, I.M.; Grilli, M.L.; Mikhaylov, A.; Senjyu, T. Green synthesis of silver oxide nanoparticles for photocatalytic environmental remediation and biomedical applications. *Metals* **2022**, *12*, 769. [CrossRef]

15. Danish, M.S.S.; Estrella, L.L.; Alemaida, I.M.A.; Lisin, A.; Moiseev, N.; Ahmadi, M.; Nazari, M.; Wali, M.; Zaheb, H.; Senjyu, T. Photocatalytic applications of metal oxides for sustainable environmental remediation. *Metals* **2021**, *11*, 80. [CrossRef]

16. Nair, G.M.; Sajini, T.; Mathew, B. Advanced green approaches for metal and metal oxide nanoparticles synthesis and their environmental applications. *Talanta* **2022**, *5*, 100080. [CrossRef]

17. Danish, M.S.S.; Bhattacharya, A.; Stepanova, D.; Mikhaylov, A.; Grilli, M.L.; Khosravy, M.; Senjyu, T. A systematic review of metal oxide applications for energy and environmental sustainability. *Metals* **2020**, *10*, 1604. [CrossRef]

18. Su, R.; Xie, C.; Alhassan, S.I.; Huang, S.; Chen, R.; Xiang, S.; Wang, Z.; Huang, L. Oxygen reduction reaction in the field of water environment for application of nanomaterials. *J. Nanomater.* **2020**, *10*, 1719. [CrossRef]

19. Abid, N.; Khan, A.M.; Shujait, S.; Chaudhary, K.; Ikram, M.; Imran, M.; Haider, J.; Khan, M.; Khan, Q.; Maqbool, M. Synthesis of nanomaterials using various top-down and bottom-up approaches, influencing factors, advantages, and disadvantages: A review. *Adv. Colloid Interface Sci.* **2021**, *300*, 102597. [CrossRef]

20. Sargazi, A.; Barani, A.; Heidari Majd, M. Synthesis and apoptotic efficacy of biosynthesized silver nanoparticles using acacia luciana flower extract in MCF-7 breast cancer cells: Activation of bak1 and bclx for cancer therapy. *BioNanoScience* **2020**, *10*, 683–689. [CrossRef]

21. de Souza, T.A.J.; Souza, L.R.R.; Franchi, L.P. Silver nanoparticles: An integrated view of green synthesis methods, transformation in the environment, and toxicity. *Ecotoxicol. Environ. Saf.* **2019**, *171*, 691–700. [CrossRef] [PubMed]

22. Galúcio, J.M.; de Souza, S.G.B.; Vasconcelos, A.A.; Lima, A.K.O.; da Costa, K.S.; de Campos Braga, H.; Taube, P.S. Synthesis, characterization, applications, and toxicity of green synthesized nanoparticles. *Curr. Pharm. Biotechnol.* **2022**, *23*, 420–443. [CrossRef] [PubMed]

23. Alizadeh, S.R.; Ebrahimzadeh, M.A. Characterization and anticancer activities of green synthesized CuO nanoparticles, A review. *Anti-Cancer Agents Med. Chem.* **2021**, *21*, 1529–1543. [CrossRef] [PubMed]

24. Ouerghi, O.; Geesi, M.H.; Riadi, Y.; Ibnouf, E.O. Limon-citrus extract as a capping/reducing agent for the synthesis of titanium dioxide nanoparticles: Characterization and antibacterial activity. *Green Chem. Lett. Rev.* **2022**, *15*, 483–490. [CrossRef]

25. Behzad, F.; Sefidgar, E.; Samadi, A.; Lin, W.; Pouladi, I.; Pi, J. An overview of zinc oxide nanoparticles produced by plant extracts for anti-tuberculosis treatments. *Curr. Med. Chem.* **2022**, *29*, 86–98. [CrossRef] [PubMed]

26. Silva, A.A.; Sousa, A.M.F.; Furtado, C.R.; Carvalho, N.M. Green magnesium oxide prepared by plant extracts: Synthesis, properties and applications. *Mater. Today Sustain.* **2022**, *20*, 100203. [CrossRef]

27. Eltaweil, A.S.; Fawzy, M.; Hosny, M.; Abd El-Monaem, E.M.; Tamer, T.M.; Omer, A.M. Green synthesis of platinum nanoparticles using Atriplex halimus leaves for potential antimicrobial, antioxidant, and catalytic applications. *Arab. J. Chem.* **2022**, *15*, 103517. [CrossRef]

28. Hashemi, Z.; Mizwari, Z.M.; Mohammadi-Aghdam, S.; Mortazavi-Derazkola, S.; Ebrahimzadeh, M.A. Sustainable green synthesis of silver nanoparticles using Sambucus ebulus phenolic extract (AgNPs@ SEE): Optimization and assessment of photocatalytic degradation of methyl orange and their in vitro antibacterial and anticancer activity. *Arab. J. Chem.* **2022**, *15*, 103525. [CrossRef]

29. Shirzadi-Ahodashti, M.; Mortazavi-Derazkola, S.; Ebrahimzadeh, M.A. Biosynthesis of noble metal nanoparticles using crataegus monogyna leaf extract (CML@ X-NPs, X = Ag, Au): Antibacterial and cytotoxic activities against breast and gastric cancer cell lines. *Surf. Interfaces* **2020**, *21*, 100697. [CrossRef]

30. Eslami, S.; Ebrahimzadeh, M.A.; Biparva, P. Green synthesis of safe zero valent iron nanoparticles by Myrtus communis leaf extract as an effective agent for reducing excessive iron in iron-overloaded mice, a thalassemia model. *RSC Adv.* **2018**, *8*, 26144–26155. [CrossRef]

31. Johnson, J.; Shanmugam, R.; Lakshmi, T. A review on plant-mediated selenium nanoparticles and its applications. *J. Popul. Ther. Clin. Pharmacol.* **2022**, *28*, e29–e40. [PubMed]

32. Ameri, A.; Shakibaie, M.; Ameri, A.; Faramarzi, M.A.; Amir-Heidari, B.; Forootanfar, H. Photocatalytic decolorization of bromothymol blue using biogenic selenium nanoparticles synthesized by terrestrial actinomycete Streptomyces griseobrunneus strain FSHH12. *Desalin. Water Treat.* **2016**, *57*, 21552–21563. [CrossRef]

33. Pouri, S.; Motamedi, H.; Honary, S.; Kazeminezhad, I. Biological synthesis of selenium nanoparticles and evaluation of their bioavailability. *Braz. Arch. Biol. Technol.* **2018**, *60*, 170452. [CrossRef]

34. Goud, K.G.; Veldurthi, N.K.; Vithal, M.; Reddy, G. Characterization and evaluation of biological and photocatalytic activities of selenium nanoparticles synthesized using yeast fermented broth. *J. Mater. NanoSci.* **2016**, *3*, 33–40.

35. Velayati, M.; Hassani, H.; Sabouri, Z.; Mostafapour, A.; Darroudi, M. Biosynthesis of Se-Nanorods using Gum Arabic (GA) and investigation of their photocatalytic and cytotoxicity effects. *Inorg. Chem. Commun.* **2021**, *128*, 108589. [CrossRef]

36. Xia, X.; Zhou, Z.; Wu, S.; Wang, D.; Zheng, S.; Wang, G. Adsorption removal of multiple dyes using biogenic selenium nanoparticles from an Escherichia coli strain overexpressed selenite reductase CsrF. *Nanomaterials* **2018**, *8*, 234. [CrossRef]

37. Santhosh, C.; Balasubramanian, B.; Vino, P.; Viji, M.; Rejeeth, C.; Kannan, S.; Ullah, H.; Rengasamy, K.R.; Daglia, M.; Maruthu-pandian, A. Biofabricated selenium nanoparticles mediated from Goniothalamus wightii gains biomedical applications and photocatalytic degrading ability. *J. King Saud Univ. Sci.* **2022**, *34*, 102331. [CrossRef]

38. Iqbal, Z.; Imran, M.; Latif, S.; Nazir, A.; Ibrahim, S.M.; Ahmad, I.; Iqbal, M.; Iqbal, S. Photocatalytic degradation of dyes in aqueous media by gum shellac stabilized selenium nanoparticles. *Z. Phys. Chem. (N F)* **2023**, *237*, 1139–1152. [CrossRef]

39. Din, M.I.; Khalid, R.; Najeeb, J.; Hussain, Z. Fundamentals and photocatalysis of methylene blue dye using various nanocatalytic assemblies—A critical review. *J. Clean. Prod.* **2021**, *298*, 126567. [CrossRef]

40. Oz, M.; Lorke, D.E.; Hasan, M.; Petroianu, G.A. Cellular and molecular actions of Methylene Blue in the nervous system. *Med. Res. Rev.* **2011**, *31*, 93–117. [CrossRef]

41. Mashkoor, F.; Nasar, A. Magsorbents: Potential candidates in wastewater treatment technology—A review on the removal of methylene blue dye. *J. Magn. Magn. Mater.* **2020**, *500*, 166408. [CrossRef]

42. Oladoye, P.; Ajiboye, T.; Omotola, E.; Oyewola, O. Methylene blue dye: Toxicity and potential elimination technology from wastewater. *Results Eng.* **2022**, *16*, 100678. [CrossRef]

43. Alagesan, V.; Venugopal, S. Green synthesis of selenium nanoparticle using leaves extract of withania somnifera and its biological applications and photocatalytic activities. *Bionanoscience* **2019**, *9*, 105–116. [CrossRef]

44. Xia, Z.M.; Liu, Y.N.; Huang, Z.; Qin, L.Z.; Lin, H.; Li, Q. A facile green approach for synthesis of selenium nanowires with visible light photocatalytic properties. *J. Nanosci. Nanotechnol.* **2019**, *19*, 156–162. [CrossRef]

45. Tripathi, R.M.; Hameed, P.; Rao, R.P.; Shrivastava, N.; Mittal, J.; Mohapatra, S. Biosynthesis of highly stable fluorescent selenium nanoparticles and the evaluation of their photocatalytic degradation of dye. *Bionanoscience* **2020**, *10*, 389–396. [CrossRef]

46. El-Sayed, E.-S.R.; Abdelhakim, H.K.; Ahmed, A.S. Solid-state fermentation for enhanced production of selenium nanoparticles by gamma-irradiated Monascus purpureus and their biological evaluation and photocatalytic activities. *Bioprocess Biosyst. Eng.* **2020**, *43*, 797–809. [CrossRef] [PubMed]

47. Kazemi, M.; Akbari, A.; Sabouri, Z.; Soleimanpour, S.; Zarrinfar, H.; Khatami, M.; Darroudi, M. Green synthesis of colloidal selenium nanoparticles in starch solutions and investigation of their photocatalytic, antimicrobial, and cytotoxicity effects. *Bioprocess Biosyst. Eng.* **2021**, *44*, 1215–1225. [CrossRef]

48. Cittrarasu, V.; Kaliannan, D.; Dharman, K.; Maluventhen, V.; Easwaran, M.; Liu, W.C.; Balasubramanian, B.; Arumugam, M. Green synthesis of selenium nanoparticles mediated from Ceropegia bulbosa Roxb extract and its cytotoxicity, antimicrobial, mosquitocidal and photocatalytic activities. *Sci. Rep.* **2021**, *11*, 1032. [CrossRef]

49. Alizadeh, S.R.; Seyedabadi, M.; Montazeri, M.; Khan, B.A.; Ebrahimzadeh, M.A. Allium paradoxum extract mediated green synthesis of SeNPs: Assessment of their anticancer, antioxidant, iron chelating activities, and antimicrobial activities against fungi, ATCC bacterial strains, Leishmania parasite, and catalytic reduction of methylene blue. *Mater. Chem. Phys.* **2023**, *296*, 127240.

50. Alizadeh, S.R.; Abbastabar, M.; Nosratabadi, M.; Ebrahimzadeh, M.A. High antimicrobial, cytotoxicity, and catalytic activities of biosynthesized selenium nanoparticles using Crocus caspius extract. *Arab. J. Chem.* **2023**, *16*, 104705. [CrossRef]

51. Ebrahimzadeh, M.A.; Moradsomarein, M.; Lalerdi, F.S.; Alizadeh, S.R. Biogenic synthesis of selenium nanoparticles using Hibiscus esculentus L. extract: Catalytic degradation of organic dye and its anticancer, antibacterial and antifungal activities. *Eur. J. Chem.* **2023**, *14*, 144–154. [CrossRef]

52. Velayutham, L.; Parvathiraja, C.; Anitha, D.C.; Mahalakshmi, K.; Jenila, M.; Gupta, J.K.; Wabaidur, S.M.; Siddiqui, M.R.; Aftab, S.; Lai, W.-C. Antibacterial and photocatalytic dye degradation activities of green synthesized nise nanoparticles from hibiscus rosa-sinensis leaf extract. *Water* **2023**, *15*, 1380. [CrossRef]

53. Yang, B.; Yang, J.; Huang, Z.; Qin, L.; Lin, H.; Li, Q. Green fabrication of large-size Cu$_2$Se hexagonal sheets with visible light photocatalytic activity. *Appl. Surf. Sci.* **2021**, *535*, 147712. [CrossRef]

54. Nouri, M.; Saray, A.M.; Azimi, H.; Yousefi, R. High solar-light photocatalytic activity of using Cu$_3$Se$_2$/rGO nanocomposites synthesized by a green co-precipitation method. *Solid State Sci.* **2017**, *73*, 7–12. [CrossRef]

55. Saray, A.M.; Azimi, H.; Shirmardi, A.; Nouri, M.; Yousefi, R. CuxSey@polyaniline core-shell nanocomposites based type-II heterostructures as high-performance photocatalytic materials. *J. Alloys Compd.* **2023**, *951*, 169827. [CrossRef]

56. Al-Gheethi, A.A.; Azhar, Q.M.; Kumar, P.S.; Yusuf, A.A.; Al-Buriahi, A.K.; Mohamed, R.M.S.R.; Al-Shaibani, M.M. Sustainable approaches for removing Rhodamine B dye using agricultural waste adsorbents: A review. *Chemosphere* **2022**, *287*, 132080. [CrossRef]

57. Saigl, Z.M. Various adsorbents for removal of rhodamine b dye: A review. *Indones. J. Chem.* **2021**, *21*, 1039–1056. [CrossRef]

58. Chiu, Y.-H.; Chang, T.-F.M.; Chen, C.-Y.; Sone, M.; Hsu, Y.-J. Mechanistic insights into photodegradation of organic dyes using heterostructure photocatalysts. *Catalysts* **2019**, *9*, 430. [CrossRef]

59. Che, L.; Dong, Y.; Wu, M.; Zhao, Y.; Liu, L.; Zhou, H. Characterization of selenite reduction by *Lysinibacillus* sp. ZYM-1 and photocatalytic performance of biogenic selenium nanospheres. *ACS Sustain. Chem. Eng.* **2017**, *5*, 2535–2543. [CrossRef]

60. Kazemi, M.; Akbari, A.; Soleimanpour, S.; Feizi, N.; Darroudi, M. The role of green reducing agents in gelatin-based synthesis of colloidal selenium nanoparticles and investigation of their antimycobacterial and photocatalytic properties. *J. Clust. Sci.* **2019**, *30*, 767–775. [CrossRef]

61. Britto, J.; Barani, P.; Vanaja, M.; Pushpalaksmi, E.; Jenson Samraj, J.; Annadurai, G. Adsorption of dyes by chitosan-selenium nanoparticles: Recent developments and adsorption mechanisms. *Nat. Environ. Pollut. Technol.* **2021**, *20*, 467–479. [CrossRef]

62. Lian, S.; Fan, S.; Yang, Y.; Yu, B.; Dai, C.; Qu, Y. Selenium nanoparticles with photocatalytic properties synthesized by residual activated sludge. *Sci. Total Environ.* **2022**, *809*, 151163. [CrossRef] [PubMed]

63. Velayati, M.; Hassani, H.; Darroudi, M. Green synthesis of Se-Nanorods using Poly Anionic Cellulose (PAC) and examination of their photocatalytic and cytotoxicity effects. *Inorg. Chem. Commun.* **2021**, *133*, 108935. [CrossRef]

64. Velayati, M.; Hassani, H.; Sabouri, Z.; Mostafapour, A.; Darroudi, M. Green-based biosynthesis of Se nanorods in chitosan and assessment of their photocatalytic and cytotoxicity effects. *Environ. Technol. Innov.* **2022**, *27*, 102610. [CrossRef]

65. Ibrahim, S.M.; Al-Hossainy, A.F.; Saha, B.; Abd El-Aal, M. Removal of bromothymol blue dye by the oxidation method using KMnO4: Accelerating the oxidation reaction by Ru (III) catalyst. *J. Mol. Struct.* **2022**, *1268*, 133679. [CrossRef]

66. Dada, E.O.; Ojo, I.A.; Alade, A.O.; Afolabi, T.J.; Jimoh, M.O.; Dauda, M.O. Biosorption of bromo-based dyes from wastewater using low-cost adsorbents: A review. *J. Sci. Res. Rep.* **2020**, *26*, 34–56. [CrossRef]

67. Raval, N.P.; Shah, P.U.; Shah, N.K. Malachite green "a cationic dye" and its removal from aqueous solution by adsorption. *Appl. Water Sci.* **2017**, *7*, 3407–3445. [CrossRef]

68. Srivastava, S.; Sinha, R.; Roy, D. Toxicological effects of malachite green. *Aquat. Toxicol.* **2004**, *66*, 319–329. [CrossRef]

69. Saied, E.; Mekky, A.E.; Al-Askar, A.A.; Hagag, A.F.; El-bana, A.A.; Ashraf, M.; Walid, A.; Nour, T.; Fawzi, M.M.; Arishi, A.A. Aspergillus terreus-mediated selenium nanoparticles and their antimicrobial and photocatalytic activities. *Crystals* **2023**, *13*, 450. [CrossRef]

70. Aliabadi, R.S.; Mahmoodi, N.O. Synthesis and characterization of polypyrrole, polyaniline nanoparticles and their nanocomposite for removal of azo dyes; sunset yellow and Congo red. *J. Clean. Prod.* **2018**, *179*, 235–245. [CrossRef]

71. Fazeli, S.; Sohrabi, B.; Tehrani-Bagha, A.R. The study of Sunset Yellow anionic dye interaction with gemini and conventional cationic surfactants in aqueous solution. *Dyes Pigm.* **2012**, *95*, 768–775. [CrossRef]

72. Rovina, K.; Prabakaran, P.P.; Siddiquee, S.; Shaarani, S.M. Methods for the analysis of Sunset Yellow FCF (E110) in food and beverage products—A review. *TrAC Trends Anal. Chem.* **2016**, *85*, 47–56. [CrossRef]

73. Hassanien, R.; Abed-Elmageed, A.A.; Husein, D.Z. Eco-friendly approach to synthesize selenium nanoparticles: Photocatalytic degradation of sunset Yellow Azo Dye and anticancer activity. *ChemistrySelect* **2019**, *4*, 9018–9026. [CrossRef]

74. Ibrahim, A.G.; Sayed, A.Z.; Abd El-Wahab, H.; Sayah, M.M. Synthesis of a hydrogel by grafting of acrylamide-co-sodium methacrylate onto chitosan for effective adsorption of Fuchsin basic dye. *Int. J. Biol. Macromol.* **2020**, *159*, 422–432. [CrossRef]

75. Jain, R.; Mendiratta, S.; Kumar, L.; Srivastava, A. Green synthesis of iron nanoparticles using Artocarpus heterophyllus peel extract and their application as a heterogeneous Fenton-like catalyst for the degradation of Fuchsin Basic dye. *Curr. Res. Green Sustain. Chem.* **2021**, *4*, 100086. [CrossRef]

76. El Haddad, M. Removal of Basic Fuchsin dye from water using mussel shell biomass waste as an adsorbent: Equilibrium, kinetics, and thermodynamics. *J. Taibah Univ. Sci.* **2016**, *10*, 664–674. [CrossRef]

77. Al Jahdaly, B.A.; Al-Radadi, N.S.; Eldin, G.M.; Almahri, A.; Ahmed, M.; Shoueir, K.; Janowska, I. Selenium nanoparticles synthesized using an eco-friendly method: Dye decolorization from aqueous solutions, cell viability, antioxidant, and antibacterial effectiveness. *J. Mater. Res. Technol.* **2021**, *11*, 85–97. [CrossRef]

78. Raval, N.P.; Shah, P.U.; Shah, N.K. Adsorptive amputation of hazardous azo dye Congo red from wastewater: A critical review. *Environ. Sci. Pollut. Res.* **2016**, *23*, 14810–14853. [CrossRef]

79. Harja, M.; Buema, G.; Bucur, D. Recent advances in removal of Congo Red dye by adsorption using an industrial waste. *Sci. Rep.* **2022**, *12*, 6087. [CrossRef]

80. Karadeniz, S.C.; Isik, B.; Ugraskan, V.; Cakar, F. Agricultural Lolium perenne seeds as a low-cost biosorbent for Safranine T adsorption from wastewater: Isotherm, kinetic, and thermodynamic studies. *Phys. Chem. Earth Parts A/B/C* **2023**, *129*, 103338. [CrossRef]

81. Gupta, V.K.; Mittal, A.; Jain, R.; Mathur, M.; Sikarwar, S. Adsorption of Safranin-T from wastewater using waste materials—Activated carbon and activated rice husks. *J. Colloid Interface Sci.* **2006**, *303*, 80–86. [CrossRef]

82. Wan, H.; Chen, H.; Chu, Y.; Ju, X.; Jiang, H. Structure characterization and optical properties investigation of the four main components of the classical phenazinium dye Safranin O. *Analyst* **2019**, *144*, 7149–7156. [CrossRef] [PubMed]

83. Aljuaid, A.; Almehmadi, M.; Alsaiari, A.A.; Allahyani, M.; Abdulaziz, O.; Alsharif, A.; Alsaiari, J.A.; Saih, M.; Alotaibi, R.T.; Khan, I. g-C3N4 Based photocatalyst for the efficient photodegradation of toxic methyl orange dye: Recent modifications and future perspectives. *Molecules* **2023**, *28*, 3199. [CrossRef] [PubMed]

84. Ahluwalia, S.; Prakash, N.T.; Prakash, R.; Pal, B. Improved degradation of methyl orange dye using bio-co-catalyst Se nanoparticles impregnated ZnS photocatalyst under UV irradiation. *Chem. Eng. J.* **2016**, *306*, 1041–1048. [CrossRef]

85. Hamza, M.A.; Rizk, S.A.; Ezz-Elregal, E.-E.M.; El-Rahman, S.A.A.; Ramadan, S.K.; Abou-Gamra, Z.M. Photosensitization of TiO$_2$ microspheres by novel Quinazoline-derivative as visible-light-harvesting antenna for enhanced Rhodamine B photodegradation. *Sci. Rep.* **2023**, *13*, 12929. [CrossRef]

86. Vigneshwaran, N.; Bharimalla, A.; Arputharaj, A. Application of functional nanoparticle finishes on cotton textiles. *Trends Text. Eng. Fashion Technol.* **2018**, *3*, 1–5.

87. El-Shazly, A.N.; El-Sayyad, G.S.; Hegazy, A.H.; Hamza, M.A.; Fathy, R.M.; El Shenawy, E.; Allam, N.K. Superior visible light antimicrobial performance of facet engineered cobalt doped TiO$_2$ mesocrystals in pathogenic bacterium and fungi. *Sci. Rep.* **2021**, *11*, 5609. [CrossRef]

88. El-Shazly, A.N.; Hegazy, A.H.; El Shenawy, E.; Hamza, M.A.; Allam, N.K. Novel facet-engineered multi-doped TiO_2 mesocrystals with unprecedented visible light photocatalytic hydrogen production. *Sol. Energy Mater. Sol. Cells* **2021**, *220*, 110825. [CrossRef]

89. Hashem, E.M.; Hamza, M.A.; El-Shazly, A.N.; Sanad, M.F.; Hassan, M.M.; Abdellatif, S.O. Investigating the UV absorption capabilities in novel Ag@ RGO/ZnO ternary nanocomposite for optoelectronic devices. *Nanotechnology* **2020**, *32*, 085701. [CrossRef]

90. Hashem, E.M.; Hamza, M.A.; El-Shazly, A.N.; Abd El-Rahman, S.A.; El-Tanany, E.M.; Mohamed, R.T.; Allam, N.K. Novel Z-Scheme/Type-II CdS@ ZnO/g-C3N4 ternary nanocomposites for the durable photodegradation of organics: Kinetic and mechanistic insights. *Chemosphere* **2021**, *277*, 128730. [CrossRef]

91. Hamza, M.A.; Abd El-Rahman, S.A.; El-Shazly, A.N.; Hashem, E.M.; Mohamed, R.T.; El-Tanany, E.M.; Elmahgary, M.G. Facile one-pot ultrasonic-assisted synthesis of novel Ag@ RGO/g-C3N4 ternary 0D@ 2D/2D nanocomposite with enhanced synergetic tandem adsorption-photocatalytic degradation of recalcitrant organic dyes: Kinetic and mechanistic insights. *Mater. Res. Bull.* **2021**, *142*, 111386. [CrossRef]

92. Ahmed, M.; Abou-Gamra, Z.; Medien, H.; Hamza, M. Effect of porphyrin on photocatalytic activity of TiO_2 nanoparticles toward Rhodamine B photodegradation. *J. Photochem. Photobiol. B Biol.* **2017**, *176*, 25–35. [CrossRef] [PubMed]

93. Hamza, M.; Abou-Gamra, Z.; Ahmed, M.; Medien, H. The critical role of Tween 80 as a 'green'template on the physical properties and photocatalytic performance of TiO_2 nanoparticles for Rhodamine B photodegradation. *J. Mater. Sci.: Mater. Electron.* **2020**, *31*, 4650–4661.

94. Cui, J.-W.; Hou, S.-X.; Van Hecke, K.; Cui, G.-H. Rigid versus semi-rigid bis (imidazole) ligands in the assembly of two Co (II) coordination polymers: Structural variability, electrochemical properties and photocatalytic behavior. *Dalton Trans.* **2017**, *46*, 2892–2903. [CrossRef]

95. Zhao, Y.; Li, L.; Liu, Z.Y.; Ding, B.; Wang, X.G.; Luo, Y.; Zhao, X.J.; Yang, E.C. Water-stable Zn (II) coordination polymers regulated by polysubstituted benzenes and their photocatalytic performance toward methylene blue degradation dominated by ligand-field effects. *Cryst. Growth Des.* **2021**, *21*, 1218–1232. [CrossRef]

96. Luo, Y.; Su, R.; Yao, H.; Zhang, A.; Xiang, S.; Huang, L. Degradation of trimethoprim by sulfate radical-based advanced oxidation processes: Kinetics, mechanisms, and effects of natural water matrices. *Environ. Sci. Pollut. Res.* **2021**, *28*, 62572–62582. [CrossRef]

97. Zuo, R.; Du, G.; Zhang, W.; Liu, L.; Liu, Y.; Mei, L.; Li, Z. Photocatalytic degradation of methylene blue using TiO_2 impregnated diatomite. *Adv. Mater. Sci. Eng.* **2014**, *2014*, 170148. [CrossRef]

98. Wang, X.Q.; Han, S.F.; Zhang, Q.W.; Zhang, N.; Zhao, D.D. In photocatalytic oxidation degradation mechanism study of methylene blue dye waste water with GR/iTiO2. *EDP Sci.* **2018**, *238*, 03006. [CrossRef]

99. Alizadeh, S.R.; Biparva, P.; Goli, H.R.; Khan, B.A.; Ebrahimzadeh, M.A. Green synthesis of AuNPs by Crocus caspius— Investigation of catalytic degradation of organic pollutants, their cytotoxicity, and antimicrobial activity. *Catalysts* **2023**, *13*, 63. [CrossRef]

100. Naz, M.; Rafiq, A.; Ikram, M.; Haider, A.; Ahmad, S.O.A.; Haider, J.; Naz, S. Elimination of dyes by catalytic reduction in the absence of light: A review. *J. Mater. Sci.* **2021**, *56*, 15572–15608. [CrossRef]

101. Šimšíková, M.; Bartoš, M.; Čechal, J.; Šikola, T. Decolorization of organic dyes by gold nanoflowers prepared on reduced graphene oxide by tea polyphenols. *Catal. Sci. Technol.* **2016**, *6*, 3008–3017. [CrossRef]

102. Liang, L.; Cheng, L.; Zhang, Y.; Wang, Q.; Wu, Q.; Xue, Y.; Meng, X. Efficiency and mechanisms of rhodamine B degradation in Fenton-like systems based on zero-valent iron. *RSC Adv.* **2020**, *10*, 28509–28515. [CrossRef]

103. Huang, Z.; Zhang, F.; Tang, Y.; Wen, Y.; Wu, Z.; Fang, Z.; Tian, X. Rapid degradation of rhodamine b through visible-photocatalytic advanced oxidation using self-degradable natural perylene quinone derivatives—Hypocrellins. *Bioengineering* **2022**, *9*, 307. [CrossRef] [PubMed]

104. Diao, Z.H.; Liu, J.J.; Hu, Y.X.; Kong, L.J.; Jiang, D.; Xu, X.R. Comparative study of Rhodamine B degradation by the systems pyrite/H_2O_2 and pyrite/persulfate: Reactivity, stability, products and mechanism. *Sep. Purif. Technol.* **2017**, *184*, 374–383. [CrossRef]

105. Bouanimba, N.; Laid, N.; Zouaghi, R.; Sehili, T. A comparative study of the activity of TiO_2 degussa P25 and millennium PCs in the photocatalytic degradation of bromothymol blue. Int. *J. Chem. React. Eng.* **2017**, *16*, 20170014. [CrossRef]

106. Ayoub, H.; Kassir, M.; Raad, M.; Bazzi, H.; Hijazi, A. Effect of dye structure on the photodegradation kinetic using TiO_2 nanoparticles. *J. Mater. Sci. Chem. Eng.* **2017**, *5*, 31–45.

107. Tahir, H.; Saad, M. Ussing dyes to evaluate the photocatalytic activity. *Interface Sci. Technol.* **2021**, *32*, 125–224.

108. Selvaraj, V.; Karthika, T.S.; Mansiya, C.; Alagar, M. An over review on recently developed techniques, mechanisms and intermediate involved in the advanced azo dye degradation for industrial applications. *J. Mol. Struct.* **2021**, *1224*, 129195. [CrossRef]

109. Chen, C.; Lu, C.; Chung, Y.; Jan, J. UV light induced photodegradation of malachite green on TiO_2 nanoparticles. *J. Hazard. Mater.* **2007**, *141*, 520–528. [CrossRef]

110. Abu-Zurayk, R.; Khalaf, A.; Abbas, H.A.; Nasr, R.A.; Jamil, T.S.; Al Bawab, A. Photodegradation of carbol fuchsin dye using an $Fe_{2-x}Cu_xZr_{2-x}W_xO_7$ photocatalyst under visible-light irradiation. *Catalysts* **2021**, *11*, 1473. [CrossRef]
111. Ray, S.K.; Dhakal, D.; Lee, S.W. Insight into malachite green degradation, mechanism and pathways by morphology-tuned α-NiMoO$_4$ photocatalyst. *J. Photochem. Photobiol.* **2018**, *94*, 552–563. [CrossRef] [PubMed]